Rock Mechanics and Rock Engineering (2020) 53:1827–1856
https://doi.org/10.1007/s00603-019-02018-w

ORIGINAL PAPER

Numerical Modeling Study of the Geo-mechanical Response of Strata in Longwall Operations with Particular Reference to Indian Geo-mining Conditions

B. Behera[1] · A. Yadav[1] · G. S. P. Singh[1] · S. K. Sharma[1]

Received: 24 February 2019 / Accepted: 14 November 2019 / Published online: 23 November 2019

Abstract
India has been seeking technology for mass production of coal below ground. Longwall technology was accepted as one of the options a few decades ago. Unfortunately, it failed to meet the expected benchmark for success. This shortfall was deciphered and attributed to the inadequate understanding of cavability, leading to a mismatch in support performances. Hence, the present study attempted to bridge the gap in understanding of the strata behavior in longwall workings for the Indian geological formations. Four longwall panels representative of the major Indian coalfields were selected for the investigation. An effort was made to supplement the design-based knowledge of longwall workings, under different geo-mining and strata conditions. The stress redistribution was observed with the progressive mining along with the model and field-observed mechanism of strata failure, caving, and support loading. The effect of mining activities on the failure and deformation characteristics of the strata was studied using Finite Difference software FLAC^{3D}. It was found that the geo-mechanical properties of the overlying strata and the depth of mining were the most influential factors in controlling the behavior of the strata. At shallow depth, mechanical strength and the thickness of the overlying strata were identified as the main controlling parameters for most of the ground control events. However, at greater depths, face instability appeared to be the major contributor to these events. It is inferred that the proposed numerical modeling approach could be effectively utilized for evaluation of the stress redistribution, mechanism of failure, quantification of caving span, face convergence, and support loading for longwall panels in Indian geo-mining conditions.

Keywords Longwall mining · Indian geo-mining conditions · Strata behavior · Numerical modeling

List of Symbols

S_c	Uniaxial compressive strength
S_t	Brazilian tensile strength
σ_h	Mean horizontal in situ stress
ν	Poisson's ratio
γ	Unit weight of the overlying rock
H	Depth of cover
β	Coefficient of linear thermal expansion
E	Elastic modulus
G	Geothermal gradient
σ_v	In situ vertical stress

Abbreviations

GCF	Godavari valley coalfields
JCF	Jharia coalfields
RCF	Raniganj coalfields
S_PCF	Sohagpur coalfields
S_tCF	Sonhat coalfields

1 Introduction

In India, the first powered support longwall was deployed in 1978 at Moonidih colliery of Bharat Coking Coal Limited (BCCL). In the past 4 decades, about 80 longwall faces were worked with support capacity up to 1152 ton with a production capacity of 3 million tons per annum under different geo-mining conditions. However, the overall performance has not been encouraging when compared with other major coal-producing countries. The major reasons cited were the inadequate characterization of the geological and

✉ G. S. P. Singh
gspsingh.min@iitbhu.ac.in

[1] Department of Mining Engineering, IIT (BHU) Varanasi, Varanasi 221005, India

geotechnical conditions, improper design of panels, and poor selection of shield capacity (Ghose and Dutta 1987; Ghosh 2003; Tadisetty et al. 2006; Islavath et al. 2016). The failure of the initial longwall projects thwarted the large-scale adoption of this technology. Some of the longwall faces at JK5, PVK, and GDK10 in Godavari Valley coalfields (GCF), Jhanjra in Raniganj coalfields (RCF), and Moonidih in Jharia coalfields (JCF) operated without any strata control problem. However, the experience at the Dhemomain and the Khottadih faces of RCF and Churcha faces of Sonhat coalfields (S_tCF) proved disastrous (Sarkar 1998; Singh and Singh 2010b; Deb and Verma 2004). The shallow depth workings of Balrampur, Rajendra, and New Kumda mines of Sohagpur coalfields (S_pCF) faced severe strata control problems due to the presence of massive main roof. These workings required induced caving by deep hole surface blasting for controlling the weighting severity (Pan and Prasad 1999; Sarkar and Dhar 1993).

Regular caving of the overlying strata is essential in longwall workings as it ensures a safe stress environment by eliminating the excessive load on the support and abutment stress around the longwall faces. Delayed caving causes dynamic loading of supports, spalling, and rock burst at the face. At times, mild-to-severe air blasts are also experienced (Shabanimashcool et al. 2014). Therefore, a careful understanding of the caving mechanism is essential at the design and planning stage for effective ground control. Through numerous analytical, empirical, and numerical approaches, researchers have studied the mechanism of the roof caving under different geo-mining conditions. Using classical beam theory, Obert and Duvall (1967) studied the mechanism of strata caving and predicted the length of the void where the first and periodic caving events would occur. Adopting the bending moment approach, Majumdar (1986) suggested the first and periodic caving spans for Indian coal measure rocks. Similarly, a series of empirical models had been developed in the past for understanding the caving behavior of the strata, based on the specific mechanical concepts or field observations. While some of these approaches suggested roof classifications for qualitative assessment of caving behavior (Zamarski 1970; Arioglu and Yuksel 1984; Zhao 1985; Peng et al. 1986, 1989), there were other models that proposed quantitative aspects to predict the caving behavior of the strata (Pawlowicz 1967; Bilinski and Konopko 1973; Singh and Singh 1979, 1982; Unrug and Szwilski 1980; Peng 2006). All the proposed approaches being site-specific were based on specific geo-mining conditions. Similarly, over the years, some numerical modeling approaches had also developed to study the underlying mechanisms of the roof cavability (Vakili and Hebblewhite 2010; Shabanimashcool and Li 2012; Khanal et al. 2012; Shabanimashcool et al. 2014; Wang et al. 2018; Le et al. 2018, 2019). Although the above approaches provide some insights into the mechanisms of roof caving, their applicability is not significant due to the complexity of the geo-mining condition and the typical geo-materials involved in the Indian geological formations.

Along with the caving behavior, the interaction of the face support with the overlying strata is equally significant for the longwall geo-mechanics. To date, numerous studies were executed to understand the fundamental mechanics of shield–strata interaction at longwall face. They include detached block theory (Wilson 1975), yielding foundation theory (Smart and Aziz 1986), the empirical nomograph-based method (Peng et al. 1987), load cycle analysis (Peng 1998), neural networks (Chen 1998), ground response curves (Medhurst and Reed 2005), and Voussoir beam theory (Qian et al. 1994). Analyses were performed through various softwares (Cheng 1998; Deb 1998; Park and Deb 1999; Sandford et al. 1999; Barczak and Conover 2002; Trueman et al. 2009; Hoyer 2012) and physical modeling also (Guo 2015; Kong et al. 2017; Yang et al. 2017, 2019). However, due to the complex nature of the overlying strata and the associated depth of mining, the applicability of the above approaches is doubtful in Indian geo-mining conditions. Thus, a detailed study of roof–support interaction with progressive face advance is required for developing site-specific and rational understanding.

The structural stability of a longwall face is another critical aspect of sustained productivity. Face instability due to excessive spalling and slabbing of coal affects its regular advance and influences face production that eventually leads to substantial economic losses. Consistent caving, safe roof–support interaction, and controlled stress environment are crucial for face stability. The reverse scenario may worsen the condition with a series of production delays. Some numerical modeling studies (Bai et al. 2015, 2016; Song and Chugh 2018; Yang et al. 2019) had been carried out in the past to understand the face instability mechanism in longwall workings. These studies stated that the concentration of abutment stresses, weighting severity, and roof-to-floor convergence were the critical parameters that control the structural stability of the longwall faces.

In recent years, the depth of coal mining in India has increased. The depth of the working in some of the mines like Adriyala and Moonidih ranges between 450 and 650 m. In the future, workings of coal might operate beyond this range. The longwall workings of the GCF, operating at moderate to large cover depths, had experienced severe face spalling during face advance, in the recent past. Given these experiences, the prevailing design approach needs to be updated to meet concurrent challenges. Unfortunately, the longwall operators in India still rely on the conventional knowledge base of strata mechanics. Its application is prone to risk in the current mining scenario. Hence, a comprehensive approach is required to enhance the current

understanding of the strata behavior, the complex rock–support interaction, and face instability in such geo-mining conditions where massive sandstone predominant in the overlying strata.

Thus, the focus of this paper lies in the study of the interrelationships of ground control parameters (stress redistribution, strata failure and caving, support loading, face convergence, and instability of longwall face) in different mining conditions for Indian rock formations. A numerical modeling approach was developed in this study using Finite Difference software FLAC^{3D} (Itasca 2015) to simulate the field-scale longwall system of extraction and study the geo-mechanical response of the strata in prevailing geological formations. The modeling results were used to classify the roof behavior with progressive face advance. Four models were studied considering the variable geo-mining conditions of past longwall panels. The modeling results were validated with the field-observed caving span and support loading. The outcome of this paper supplements the existing knowledge of longwall geo-mechanics pertinent to Indian strata formations. Furthermore, it is expected to contribute to the scientific design of future longwall panels in challenging geo-mining conditions.

2 Geological Formation and Strata Behavior Experiences

The geological column above an underground working plays a significant role in the design of a safe and reliable structure. Characterization of overlying strata and its rock mass properties are crucial for the effective design of underground workings. Since longwall mining deals with large extraction below ground, a thorough knowledge of the local geology is essential to ensure safe and consistent operation. There are ample instances worldwide where the poor characterization of overlying strata led to tragic experiences (Henderson 1980; Frith and Creech 1997; Sarkar 1998; Verma and Deb 2010; Yu 2014; Verma et al. 2016; Li et al. 2018). Sarkar (1998) carried out a study of 50 different mining sites belonging to JCF, RCF, S_PCF, and GCF for developing an understanding of strata characteristics and effective design of longwall structures. The study included the percentage of sandstone content, RQD, and compressive strength to characterize the rock materials overlying the coal seams up to ten times the extraction height.

Sarkar (1998) reported that the sandstone content in RCF varied from 27 to 100%, with an average of 70%. For JCF, the average value was found to be 44%. Similarly, in S_PCF and GCF, the average sandstone contents were 87 and 90%, respectively. The value of RQD varied from 38 to 95% in RCF and JCF. In the case of S_PCF, the RQD of massive sandstone roof varied from 75 to 80%, whereas the RQD of sandstone was 70% in almost 90% of the cases in GCF (Sarkar 1998; Banerjee et al. 2016). The average compressive strength of the overlying strata in JCF varied from 39 to 80 MPa, while it ranged between 60 and 90 MPa in RCF. In S_PCF, the compressive strength varied from 7 to 49 MPa, and in GCF, it varied from 10 to 40 MPa.

The data collected from different mine sites reflect that the depth of workings of different longwall faces varied from 40 to 650 m, whereas the height of extraction ranged between 1.8 and 4.5 m. The capacity of powered roof support varied between 325 t (Moonidih face) and 1152 t (Adriyala face), out of which most of the powered supports were the four-legged chock-shield type. The caving characteristics of the strata altered from RCF to GCF. At Jhanjra mine, the shallow depth panels in RVII seam were extracted successfully without any strata control problem, whereas the longwall workings of Pasang seam in Balarampur, New Kumuda, and Bishrampur mines, and Burhar VIB seam of Rajendra mine in Sohagpur coalfield experienced severe strata control problems, during major caving while working under 50–100 m cover depth (Singh and Singh 2010b). At 150 m depth, a few faces of RVIIA seam of MIC portion of Jhanjra mine were extracted without any strata control problem. However, significant ground control challenges were observed due to deterioration of the roof followed by excessive face convergence during periods of major strata cavings in the Incline-1 portion. Longwall panels 1 and 2 of Samla seam at Khottadih mine had extremely adverse strata control condition at a cover depth of 160–190 m. This caused prolonged dynamic loading on the supports at the face. Consequently, panel 3 of the mine collapsed at 791 m of face advance due to the damage of 55 shield supports and formation of the face cavity attributed to excessive support loading. Similarly, in Churcha mine at the depth of 218 m, the face collapsed after 198 m of face advance due to uncontrolled caving (Sarkar 1998).

The strata control scenario of longwall operations at the GCF had mixed experiences. The intensity of caving was found minimal under 6–7 m thick and easily cavable immediate roofs, while the weighting severity was significant under sandstone roof with poor caving characteristics. The primary issue had been the selection of the face length. The behavior of the strata changed considerably with the variation in the length of the faces. Faces of shorter length (60–90 m) were mined out successfully without any strata control problems. However, the roof control issues were observed with longer lengths of faces (120–150 m). Frequent breakdowns of the machinery, maintenance difficulties, and production halts were experienced during the major weightings. Face spalling and cavity formations were observed due to the higher extraction heights and the presence of weak immediate roofs in GDK-11A, JK-5, and VK-7 mines (Deb and Verma 2004).

The span of roof caving observed during the main fall varied from 25 m (Panel A4 in XVIII seam, Moonidih mine) to 140 m (Panel 1 in seam V, Churcha mine). The faces at Churcha, Khottadih, Balarampur, New Kumda, Rajendra, and the GDK 9 mines experienced dynamic loading on the supports, during major caving of the strata. Here, due to the deterioration of roofs, excessive face convergence and support closure were followed with the mechanical damage of the support (Singh and Singh 2010b).

3 Description of the Study Sites

Four longwall panels belonging to different coalfields and strata conditions were considered for the numerical modeling study to analyze the strata behavior. Using the Roof Separation Index (RSI), the rock beds above the working seams were classified for the immediate roof, main roof, and overburden depending on the strata sequence and the height of extractions (Singh and Singh 2004). The height of caving was considered up to 12–15 times the extraction height after analyzing the nature of the caving of the Indian coal measure rocks.

The longwall face of Working 'A' was extracted under 392 m depth with 95 m face length and 2.5 m mining height. Four-legged powered roof supports of capacity 325 t were used during the extraction of the panel. The immediate roof primarily comprised of intercalation and shaly coal. The main roof consisted of medium to coarse grain sandstone with intercalation (Fig. 1a). The thickness of the immediate roof and the main roof was 5.6 m and 15.5 m, respectively. The compressive strength of the strata varied between 10.2 and 44.7 MPa. The tensile strength varied between 0.2 and 4.4 MPa. The lower RQD of rock beds indicated the layered nature of the strata formations that facilitated easy caving conditions.

The longwall face of Working 'B' was extracted under the 212 m depth of cover with the support capacity of 4 × 760 t. The longwall panel with 150 m face length was extracted for 3 m extraction height, partly under sandstone and partly under shaly coal immediate roof. The thickness of the immediate roof and the main roof was 30 m and 15.94 m, respectively. The low compressive strength and tensile strength of the rock beds indicated weak strata formations compared to the other sites.

The 150 m longwall face of Working 'C' was operated for 2.4 m extraction height under 53 m cover depth using powered roof supports of 4 × 450 t. The thickness of the hardcover varied from 24 to 38.55 m. The immediate roof over the coal seam consisted of medium-grained sandstone with laminated shale layers, that had the tendency of quick separation. The compressive strength of overlying rock beds varied between 8 and 23.8 MPa. The tensile strength varied from 0.08 to 2.5 MPa.

The longwall face of Working 'D' was extracted with 120 m face length and 2.2 m extraction height using 4 × 550 t supports. The overlying strata comprised of 40 m hardcover overlain by 60 m of distressed goaf of the upper seam workings. The RQD of the caving roof varied from 77 to 90%. The compressive strength of the strata varied from 30.5 to 46 MPa and the tensile strength varied from 3.3 to 5.2 MPa. The detailed lithology and the physicomechanical properties of the different rock beds of the four study sites are depicted in Fig. 1a–d.

4 Numerical Modeling Approach and Its Field Validation

An elastoplastic plain strain model was constructed in FLAC^{3D} to simulate the strata behavior of the selected longwall panels. The total length of the model was 1000 m, which is five times the length of the mining zone. The geometry of the model comprised of the floor, coal seam, and overlying roof layers up to the surface. The base of the model was fixed with rigid boundary conditions, while the roller boundary was prescribed on the other two sides. The zone size in x-, y-, and z-direction was taken as 1 m, 0.75 m, and 0.43 m, respectively, at the coal seam level. The size of the elements in the mining zone was kept equal in the coal seam but was allowed to increase in geometric progression series, maintaining a ratio of 1.1 in the roof and the floor and a ratio of 1.15 laterally. Any abrupt change in zone size was avoided to ensure the minimal influence of zones on model behavior (Fig. 2). The behavior of the sub-horizontal parting plane was simulated using interface elements characterized by Coulomb sliding and separation in tension. The interface elements were assigned values of pre-defined normal and shear stiffness in addition to joint friction, cohesion, and tension. The stiffness values of the interface elements were decided from the empirical relation as prescribed in the software manual. This was further refined by verifying the penetration rate to an acceptable limit of 10% of the minimum zone size for the value of the vertical stress prevailing in the given condition. The initial model was constructed in two stages. In the first stage, the model was solved elastically for the initialization of pre-mining stresses. In the second stage, Mohr–Coulomb plasticity material properties were assigned to represent the in situ condition of the panel. For the initialization of the in situ stress conditions, the following equations were used in the absence of field data (Sheorey 1994; Sheorey et al. 2001):

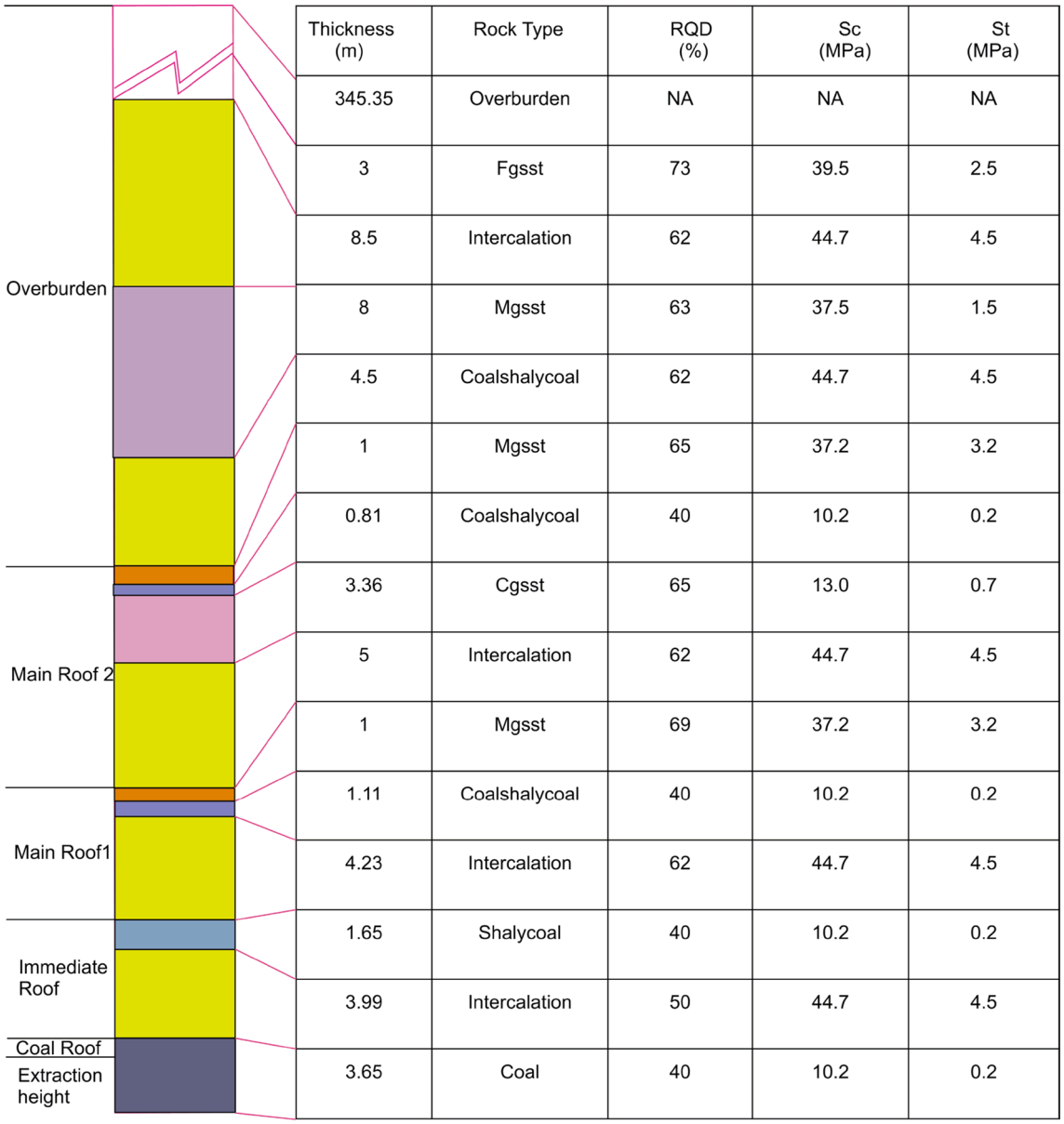

Thickness (m)	Rock Type	RQD (%)	Sc (MPa)	St (MPa)
345.35	Overburden	NA	NA	NA
3	Fgsst	73	39.5	2.5
8.5	Intercalation	62	44.7	4.5
8	Mgsst	63	37.5	1.5
4.5	Coalshalycoal	62	44.7	4.5
1	Mgsst	65	37.2	3.2
0.81	Coalshalycoal	40	10.2	0.2
3.36	Cgsst	65	13.0	0.7
5	Intercalation	62	44.7	4.5
1	Mgsst	69	37.2	3.2
1.11	Coalshalycoal	40	10.2	0.2
4.23	Intercalation	62	44.7	4.5
1.65	Shalycoal	40	10.2	0.2
3.99	Intercalation	50	44.7	4.5
3.65	Coal	40	10.2	0.2

Fig. 1 Stratigraphy and physicomechanical properties of Workings 'A', 'B', 'C', and 'D'

$$\sigma_h = \frac{\nu}{1-\nu}\gamma H + \frac{\beta E G}{1-\nu}(H + 1000), \quad ([1])$$

$$\sigma_v = \gamma H, \quad ([2])$$

where σ_h is the mean horizontal in situ stress; σ_v is the in situ vertical stress; ν is the Poisson's ratio of rock; γ is unit weight of the overlying rock, MN/m^3; H is the depth of cover, m; β is the thermal expansion coefficient of rock; 8×10^{-6}/°C for sandstone and 30×10^{-6}/°C for coal; E is Young's modulus of rock, MPa; and G is the geothermal gradient for Indian coalfields; 0.03 °C/m.

The rock mass compressive and tensile strengths of the strata were obtained from downgrading the laboratory strengths by considering scale effect and the RQD of the strata. This approach provides a good agreement for the estimation of rock mass properties in Indian coal measure rocks (Singh and Singh 2010a, b). The value of elastic modulus (E) was estimated following the approach suggested by Wilson (1980). In the absence of the tri-axial test data, the cohesive strength of different layers was derived from the rock mass UCS and the friction angle using the Mohr–Coulomb failure criterion and assuming the angle of internal friction of 25° for coal and 40° for sandstone (Singh and Singh 2009,

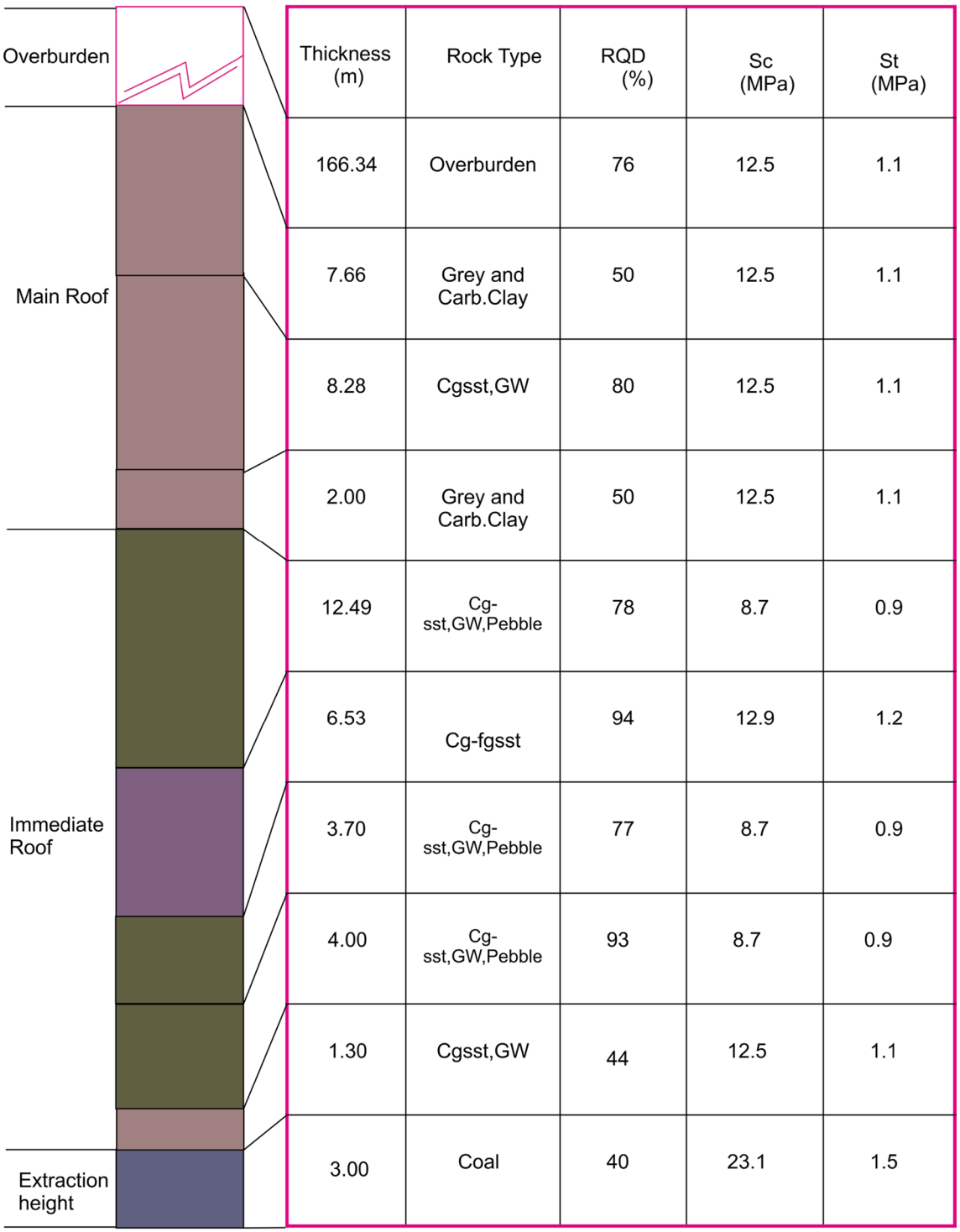

Thickness (m)	Rock Type	RQD (%)	Sc (MPa)	St (MPa)
166.34	Overburden	76	12.5	1.1
7.66	Grey and Carb.Clay	50	12.5	1.1
8.28	Cgsst,GW	80	12.5	1.1
2.00	Grey and Carb.Clay	50	12.5	1.1
12.49	Cg-sst,GW,Pebble	78	8.7	0.9
6.53	Cg-fgsst	94	12.9	1.2
3.70	Cg-sst,GW,Pebble	77	8.7	0.9
4.00	Cg-sst,GW,Pebble	93	8.7	0.9
1.30	Cgsst,GW	44	12.5	1.1
3.00	Coal	40	23.1	1.5

Fig. 1 (continued)

2010a, b). The rock mass properties used in the models are given in Table 1.

The simulation scheme for the four study sites is conceptually based on the approach suggested by Singh and Singh (2009) for the assessment of strata behavior in longwall workings. The Mohr–Coulomb plasticity model was used to capture the failure mechanism of the strata with progressive mining. The residual cohesive strength

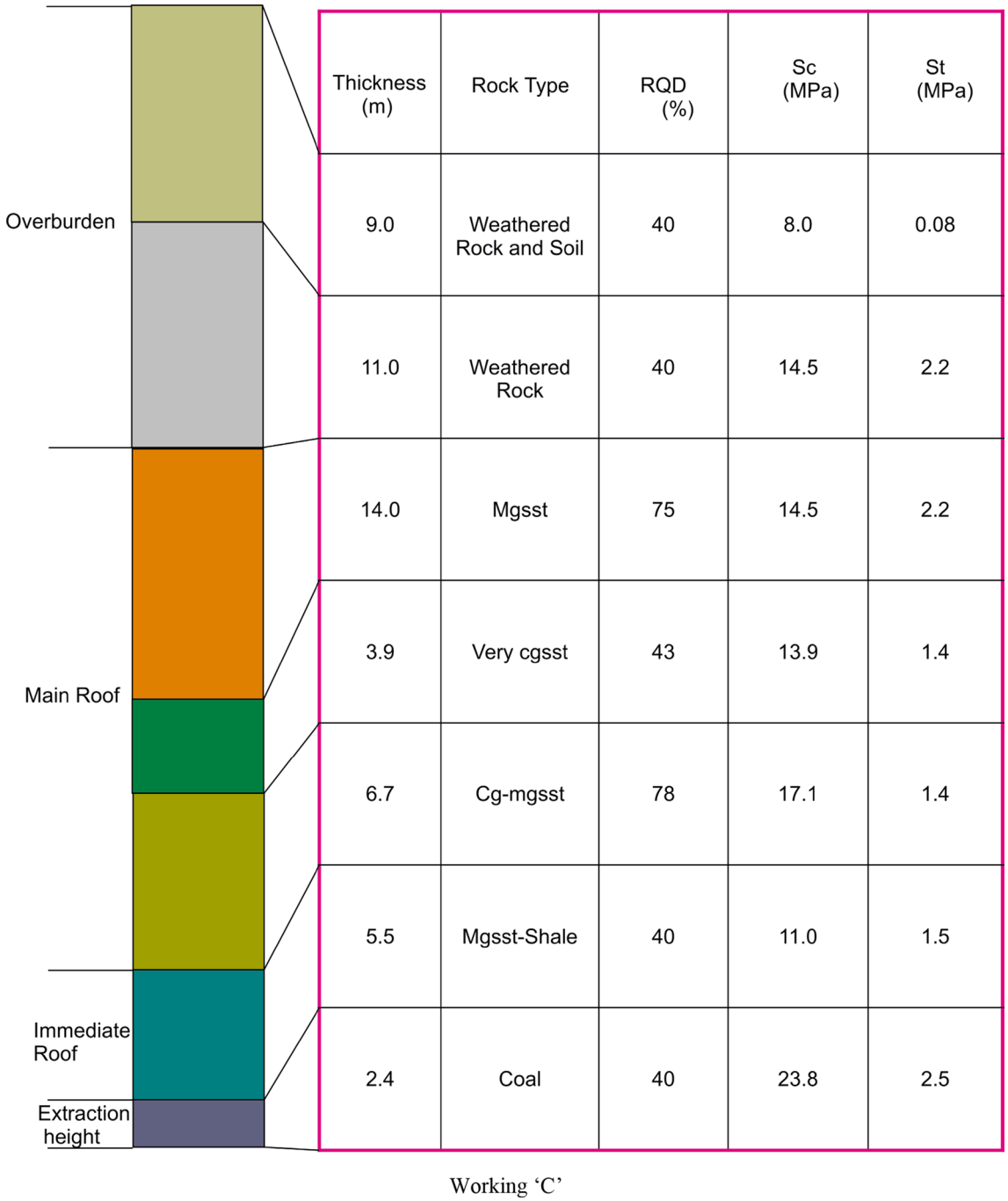

Thickness (m)	Rock Type	RQD (%)	Sc (MPa)	St (MPa)
9.0	Weathered Rock and Soil	40	8.0	0.08
11.0	Weathered Rock	40	14.5	2.2
14.0	Mgsst	75	14.5	2.2
3.9	Very cgsst	43	13.9	1.4
6.7	Cg-mgsst	78	17.1	1.4
5.5	Mgsst-Shale	40	11.0	1.5
2.4	Coal	40	23.8	2.5

Fig. 1 (continued)

was assigned as 0.8 times of the initial cohesive strength, while the residual tensile strength was assigned as zero to simulate the softening behavior of the material after failure. The concept of the ground response curve was incorporated for the cyclic installation and withdrawal of the supports during the simulation. The concept is based on the relationship of support pressure and roof convergence subjected to a dynamically changing rock environment where the excavation has been made. The interdependence of rock mass properties, support pressure, support stiffness, and ground deformation is commonly represented by ground characteristic lines and support reaction lines, as shown in Fig. 3. The portion AB of the round response curve represents the initial roof convergence, which is due to the elastic deformation of the strata that takes place immediately after the excavation of rock. The support

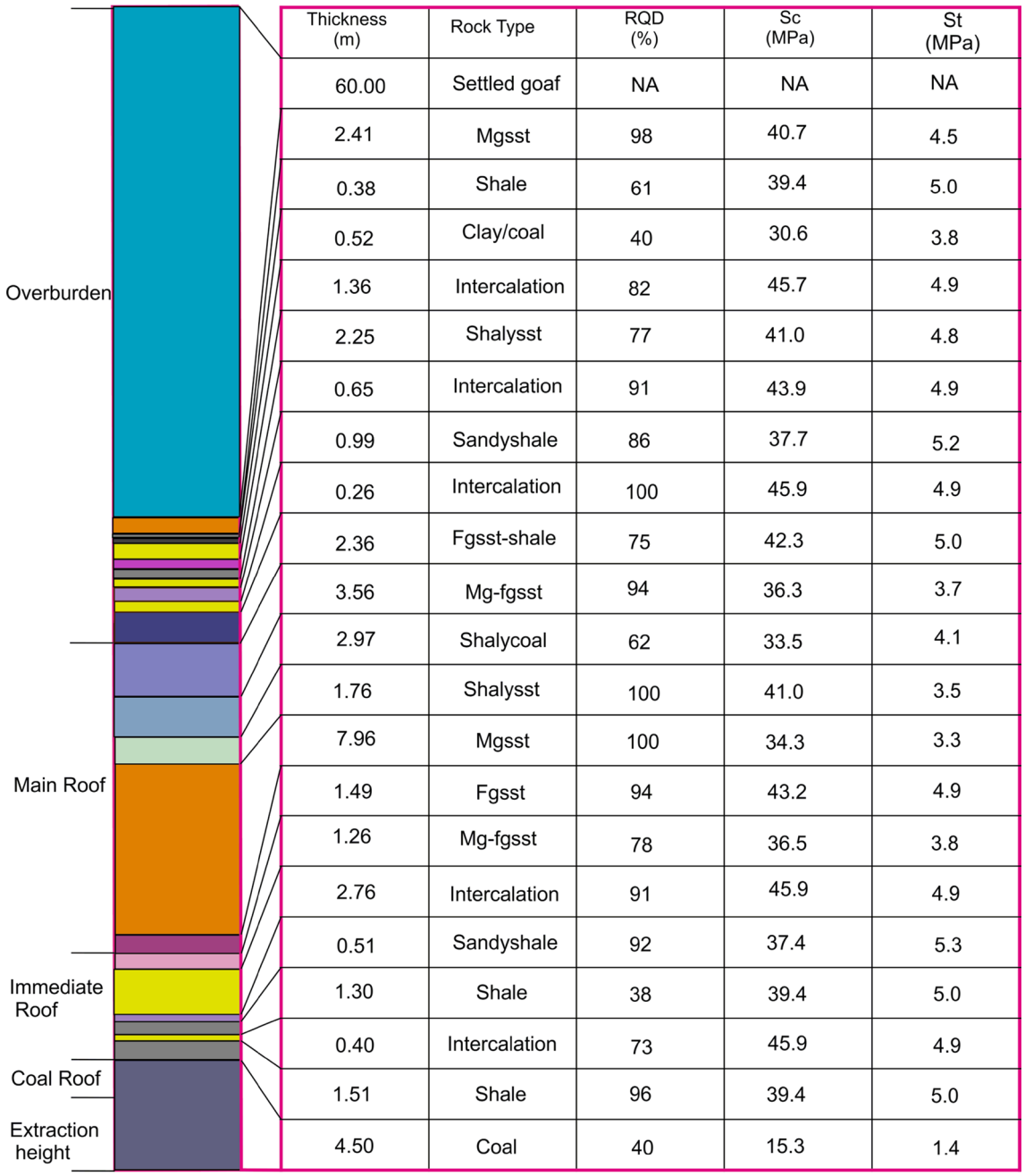

Thickness (m)	Rock Type	RQD (%)	Sc (MPa)	St (MPa)
60.00	Settled goaf	NA	NA	NA
2.41	Mgsst	98	40.7	4.5
0.38	Shale	61	39.4	5.0
0.52	Clay/coal	40	30.6	3.8
1.36	Intercalation	82	45.7	4.9
2.25	Shalysst	77	41.0	4.8
0.65	Intercalation	91	43.9	4.9
0.99	Sandyshale	86	37.7	5.2
0.26	Intercalation	100	45.9	4.9
2.36	Fgsst-shale	75	42.3	5.0
3.56	Mg-fgsst	94	36.3	3.7
2.97	Shalycoal	62	33.5	4.1
1.76	Shalysst	100	41.0	3.5
7.96	Mgsst	100	34.3	3.3
1.49	Fgsst	94	43.2	4.9
1.26	Mg-fgsst	78	36.5	3.8
2.76	Intercalation	91	45.9	4.9
0.51	Sandyshale	92	37.4	5.3
1.30	Shale	38	39.4	5.0
0.40	Intercalation	73	45.9	4.9
1.51	Shale	96	39.4	5.0
4.50	Coal	40	15.3	1.4

Working 'D'

Fig. 1 (continued)

pressure required to restrain convergence is very high in this condition, and it should match with the existing stress level. As the roof deforms, the support resistance required to prevent further convergence reduces, as arching and self-supporting capacity of the ground is induced at point B. As the roof failure initiates with further deformation, the required support resistance starts to increase with the loss of the self-supporting capability of the ground. As a result, support of higher capacity is required to contain the failed ground at point D.

In the current model, the convergence curve of the roof was obtained concerning the iteration time-steps of the numerical model to obtain a reasonable response in terms of load on the face support (Fig. 4). It was noted that the installation of support between time-steps P2 and P3 was beneficial for reducing the rate of plastic convergence, so

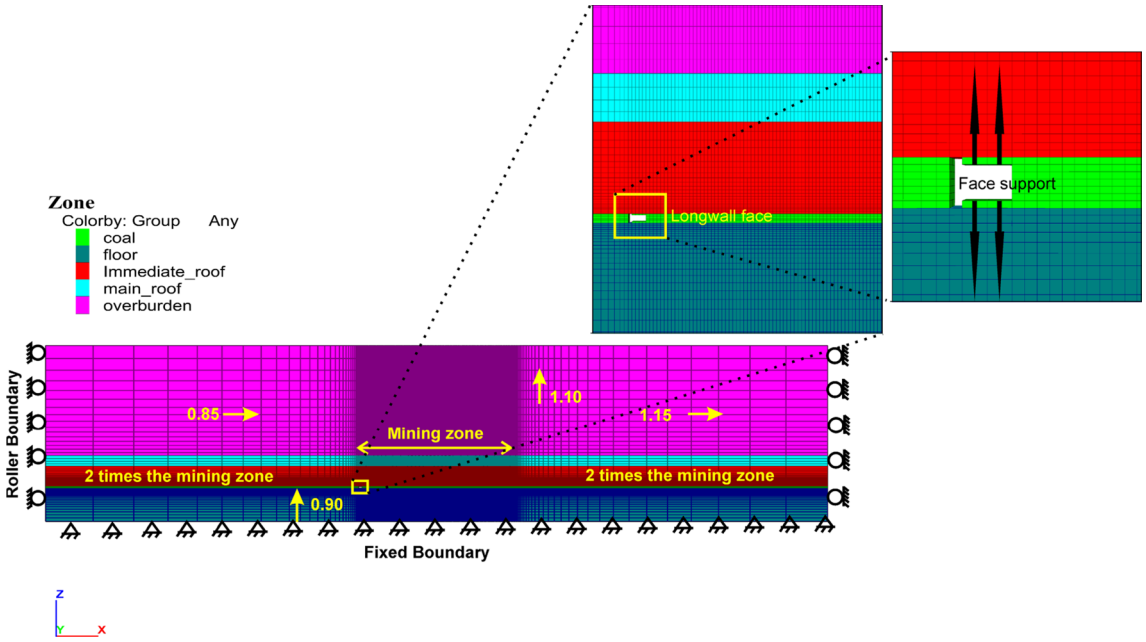

Fig. 2 A geometric view of the model

that the roof condition at the face remains stable. Therefore, the support was installed at point P2 after each stage of cyclic face advance simulated at an interval of 1 m to avoid the effect of elastic roof convergence on the support. This process ensures a field representative simulation of support loading irrespective of the depth of cover. The longwall shield was modeled by taking four elements, each along the roof and the floor of the face designated as 'canopy' and 'base' of the support, respectively. The reaction member of the support was applied at 1 m (Pt1_ars) and 3 m (Pt3_ars) behind the face, representing hydraulic legs of the support. The total load on the support was obtained as the summation of the load of the members with the progressive advance of the face (Pt1_ars and Pt3_ars) with due consideration of the two-dimensional plane strain condition, which agrees quite well with the field measurement data. The progressive load on the support was monitored through the application of '*History*' command against the time-steps of the model. The schematic representation of the simulated support and the '*History*' locations are shown in Fig. 5.

The progressive mining of the longwall face was simulated in stages of 1 m until the major caving occurs. After setting of installation chamber of 5 m width, supports of rated capacity were installed in the face with pre-defined setting and yield pressure and associated stiffness properties. A FISH routine was used to facilitate the progressive mining and advancing of the support. Removal of supports from the previous position and its installation in the new face position was controlled by an FISH routine which uses a *Ground Response Curve* to allow the rock to converge elastically before the support was deployed in the advance position and remained installed at the new face location till a stable convergence was obtained. In all the models, support was set to 60% of the yield load capacity to represent the actual field condition.

Four model indicators were used through different FISH routines to monitor the behavior of strata with progressive face advance. The model indicators are 'Front abutment stress (MPa)', 'Load on the support (*t*)', 'Face convergence slope (mm/m)', and 'failure state of the overlying strata and face'. The front abutment stress was measured at the center of the coal face using a FISH routine, which searches for the maximum value of the induced vertical stress in the coal seam up to 20 m ahead of the face line. The value of the front abutment stress was obtained in every step and stored in a particular log file. Accordingly, a term named *Vertical Stress Concentration Factor (VSCF)* was used in this paper, which is the ratio of peak mining stress (induced stress) to the pre-mining stress (in situ stress) in a given stress environment. The load on the support was estimated through the total nodal reaction exerted by the support member during each mining cycle using another FISH routine.

The convergence slope was calculated by taking the difference of the *Z*-position of the roof-level node to the corresponding floor-level node at the face. A FISH routine was used to measure face convergence for nodes located at 0, 1, 2, 3, and 4 m distance from the face during its progressive advance. The convergence slope was calculated with respect to the node at the face (0 m position) for the nodes located at 1, 2, 3, and 4 m away from the face line, and was averaged

Table 1 Rock mass properties of Working 'A', Working 'B', Working 'C', and Working 'D' considered in the model

	Thickness (m)	Density kg/m^3	Shear Mod. (GPa)	Bulk Mod. (GPa)	Tensile strength (MPa)	Cohesion (MPa)
Working 'A'						
Floor	50.0	1935	2.48	4.14	1.03	2.52
Coal	2.5	1406	0.80	1.33	0.04	0.65
Coal roof	1.15	1406	0.80	1.33	0.04	0.65
Immediate roof	5.64	1879	2.03	3.38	0.76	1.90
Main roof 1	5.34	1935	2.48	4.14	1.03	2.52
Main roof 2	10.17	2003	2.42	4.03	0.86	2.22
Overburden	370.5	2144	5.11	8.51	1.03	3.08
Working 'B'						
Floor	50.0	2300	1.54	2.57	0.35	0.96
Coal	3.0	1400	0.80	1.33	0.31	1.48
Immediate roof	30	2045	1.20	2.01	0.39	0.94
Main roof	15.94	2050	1.54	2.57	0.35	0.96
Overburden	166.34	2050	1.54	2.57	0.41	1.11
Working 'C'						
Floor	50.0	2300	1.86	3.11	0.66	1.25
Coal	2.4	1400	0.80	1.33	0.50	1.52
Immediate roof	5.5	2024	1.20	2.00	0.30	0.51
Main roof	24.6	2021	1.86	3.11	0.66	1.25
Overburden	20	1789	1.32	2.19	0.25	0.54
Working 'D'						
Floor	50.0	2300	4.89	8.15	1.98	3.97
Coal	2.4	1394	0.80	1.33	0.27	0.98
Coal roof	2.1	1394	0.80	1.33	0.27	0.98
Immediate roof	6.53	2349	5.22	8.69	1.92	3.79
Main roof	15.44	2276	3.63	6.05	1.70	3.66
Overburden	18.18	2336	4.89	8.15	1.98	3.97
Settled goaf	60	2000	0.48	0.80	0.27	0.98

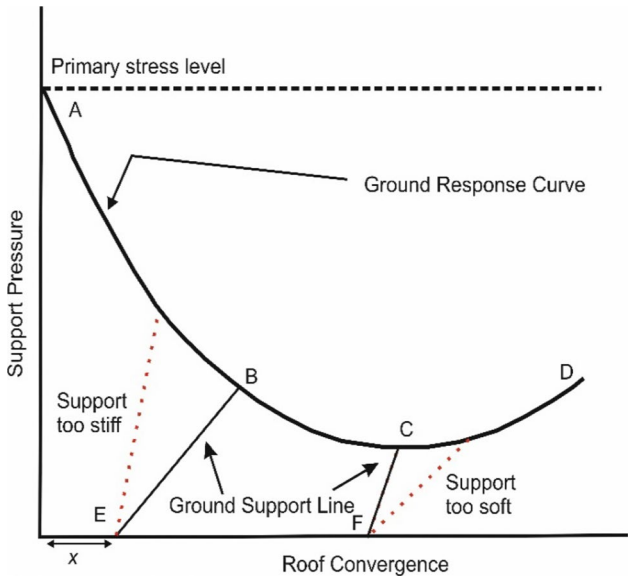

Fig. 3 Rock–support interaction diagram

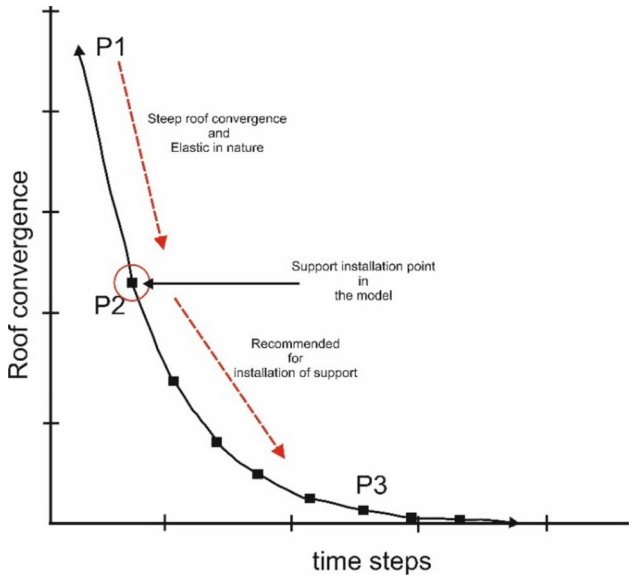

Fig. 4 Numerical model obtained ground response vs. time-stepping curve for roof strata

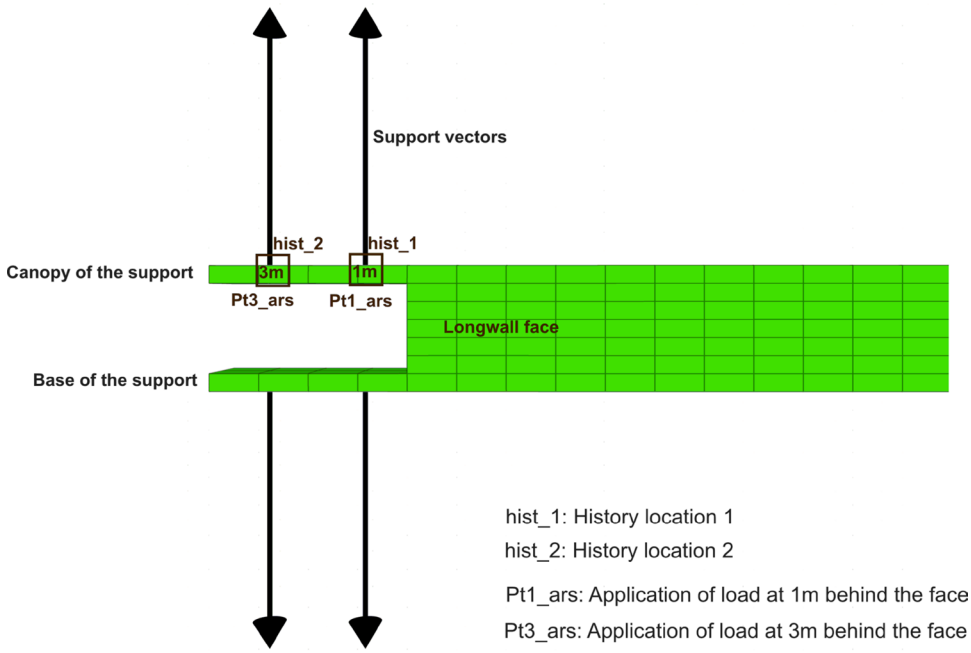

Fig. 5 Schematic diagram of modeled powered roof support with history locations

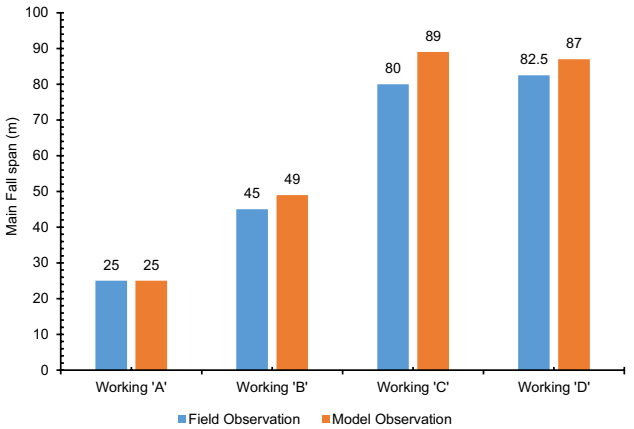

Fig. 6 Field and model observations of the main fall span of different workings

to get final convergence slope for a particular face position. The failure state of the overlying strata and the longwall face were also observed using failure state indicator flags.

The model was validated against the main fall span and load on the powered roof support observed in the middle zone of the face. The comparative plot of the span of the main fall observed in the field, and the model is shown in Fig. 6. The results obtained from the model are in close agreement with the field experience. Similarly, the correlation between the trend of loading of powered roof support observed in the field, and the model is also in close agreement (Fig. 7). In all the cases, the load on the support increased initially and then relaxed after reaching peak load during the first major caving of the main roof. The deviation of the modeled and measured support load behavior as observed in the case Workings 'B' and 'D' is likely due to the time-lapse in the manual recording of the data, which could not be incorporated in the model.

5 Simulation Results

Following basic verification of the modeling results with the field experience, an in-depth analysis of stress redistribution, failure and caving of the strata, cycling loading of the face support, and progressive face convergence as well as face instability was carried out to develop a broader understanding of the subjects.

5.1 Stress Redistribution

During underground excavation, the state of stress is disturbed and redistributed elsewhere in the surrounding rock mass. Knowledge of newly formed stress trajectory including the stress concentration as well as relaxation is critically essential to understand the mechanism of failure (Peng 2006; Rezaei et al. 2015a, b; Suchowerska et al. 2013, 2014). Before extraction, the vertical and the horizontal stresses presented the major and minor principal stresses for Workings 'A' and 'B', whereas a reverse condition was observed in case of Workings 'C' and 'D' owing to the different mining depth and elasticity properties of the overlying rock beds. In the pre-mining period, the magnitude of the major and the minor principal stresses were 8.2 and 5.6 MPa for

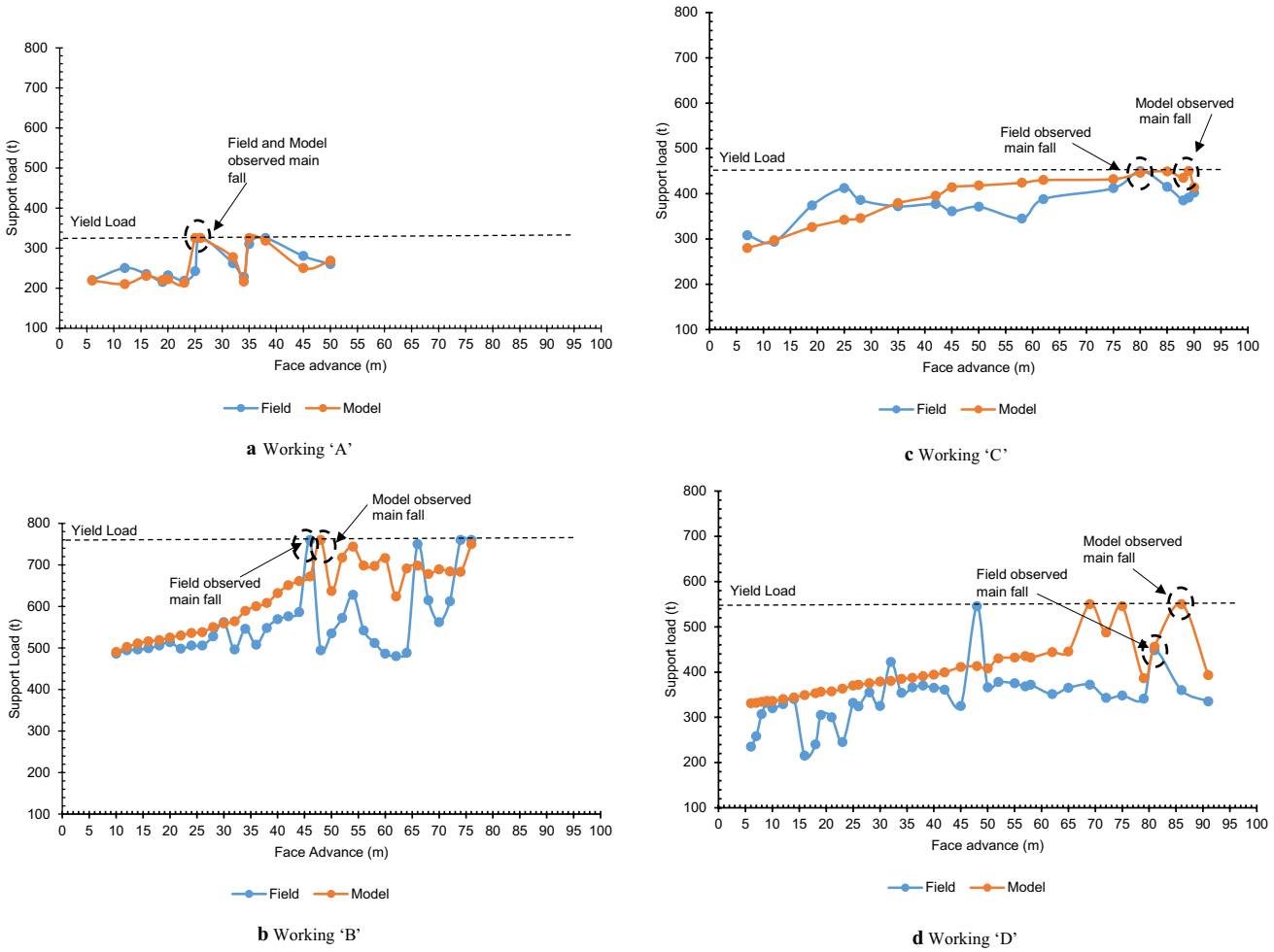

Fig. 7 Computed load and field load on the support

Working 'A', 4.3 and 3.8 MPa for Working 'B', 2.4 and 0.96 MPa for Working 'C', and 2.8 and 2.2 MPa for Working 'D', respectively. After the development of the panel, the peak value of major principal stresses concentrated at 4–5 m ahead of the extraction face in case of Working 'A', whereas it was within 1–3 m in Working 'B'. In contrast, the peak value of major principal stresses concentrated in the immediate roof and floor in case of Working 'C' and Working 'D.' The ultimate magnitude of major principal stress was experienced just before the rupture of the main roof for all the four cases (Fig. 8).

In response to the mining activity, the vertical stress relieved behind the coal face but concentrated in the unmined area ahead of the face, whereas the horizontal stress concentrated in the upper-to-lower end of immediate and main roof (Fig. 9). The peak horizontal stress was experienced at the upper end of the roof layers before caving, which was reduced after the caving occurred and was then transferred to the roof layers ahead of the face. The observation of stress distribution with the progressive advance of the face provides good agreement with the typical longwall geo-mechanics (Peng 2006; Kang et al. 2018).

The distribution of vertical stress on the floor, roof, and face of all the four workings during peak abutment period is shown in Fig. 10. It was observed that the stress relieved zone behind the face gradually increased in lateral as well as vertical direction with the progressive advance of the face. Similarly, the abutment stress concentration ahead of the face was also increased until the occurrence of the main roof caving.

In general, the height of the stress relieved zone (h_{st}) in the goaf progressively increased with the advance of the face (f_a), but this also led to a higher concentration of stress at the face because of the formation of large overhang behind the face. In Working 'A,' the stress relieved zone reached up to 20 m in the roof before caving of the main roof. Similarly, the stress relieved zone extended up to 31, 18, and 42 m at sites 'B', 'C', and 'D', respectively. These observations were primarily attributed to large overhang in Workings 'B' and 'D'. A comparatively smaller value of the h_{st}/f_a ratio

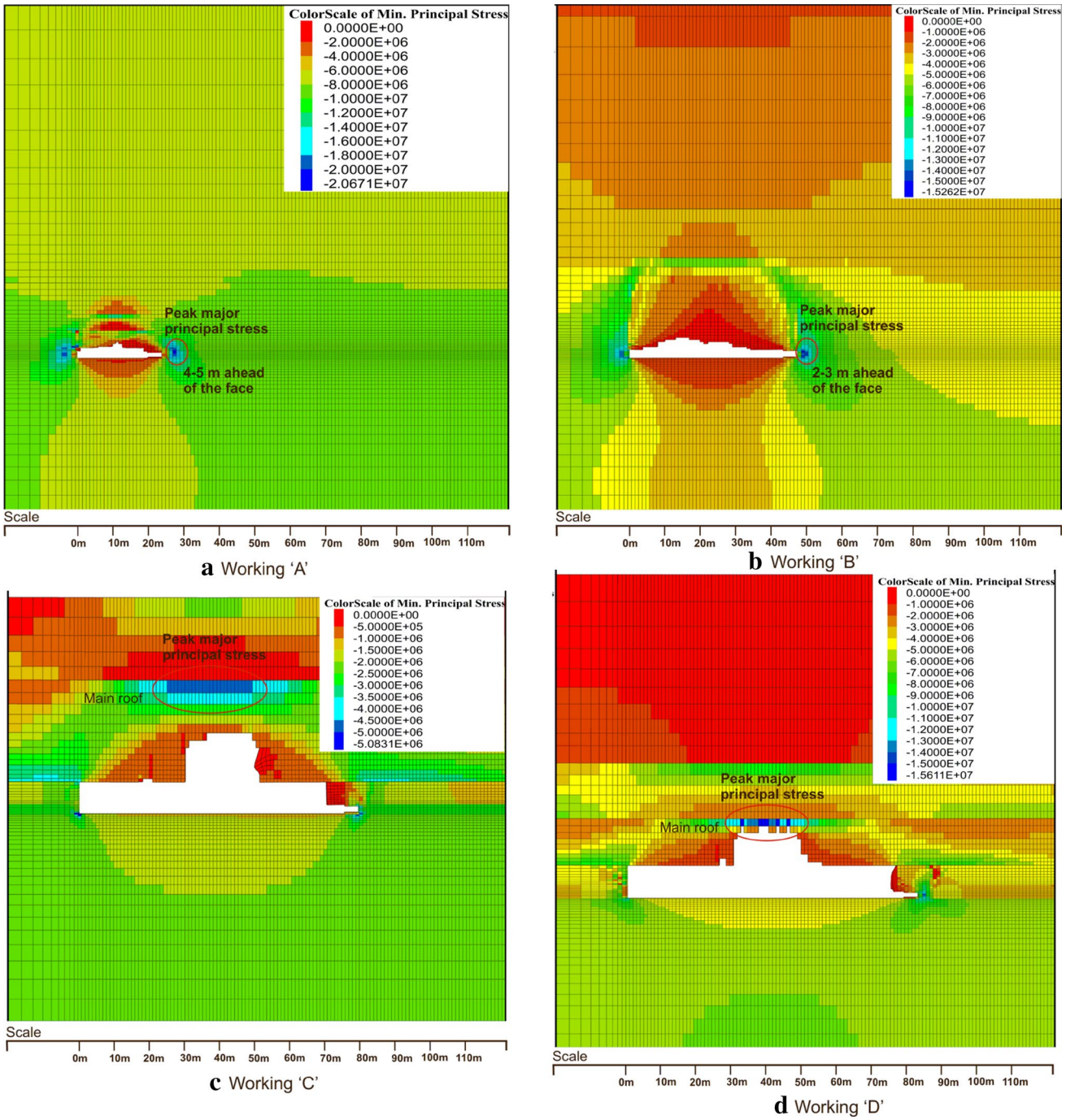

Fig. 8 Location and magnitude of peak major principal stresses just before the main fall

indicated delayed roof caving and increased the severity of impending roof weighting in general (Table 2).

The magnitude of peak abutment stress in terms of vertical stress concentration factor (VSCF) with the progressive face advance is presented in Fig. 11. The plot shows that the concentration of vertical stress rose gradually till the rupture of the overhang formed in the goaf. In Working 'A', the peak VSCF of 1.86 was found at 24 m of face advance, which was relaxed after subsequent caving of the overlying strata. Similarly, in Workings 'B', 'C', and 'D', the peak VSCF of 2.44, 1.55, and 3.94 were observed 2–5 m ahead of the face at 48, 39, and 82 m face advance, which is a valid outcome for Indian geo-mining conditions (Singh and Singh 2009, 2010b).

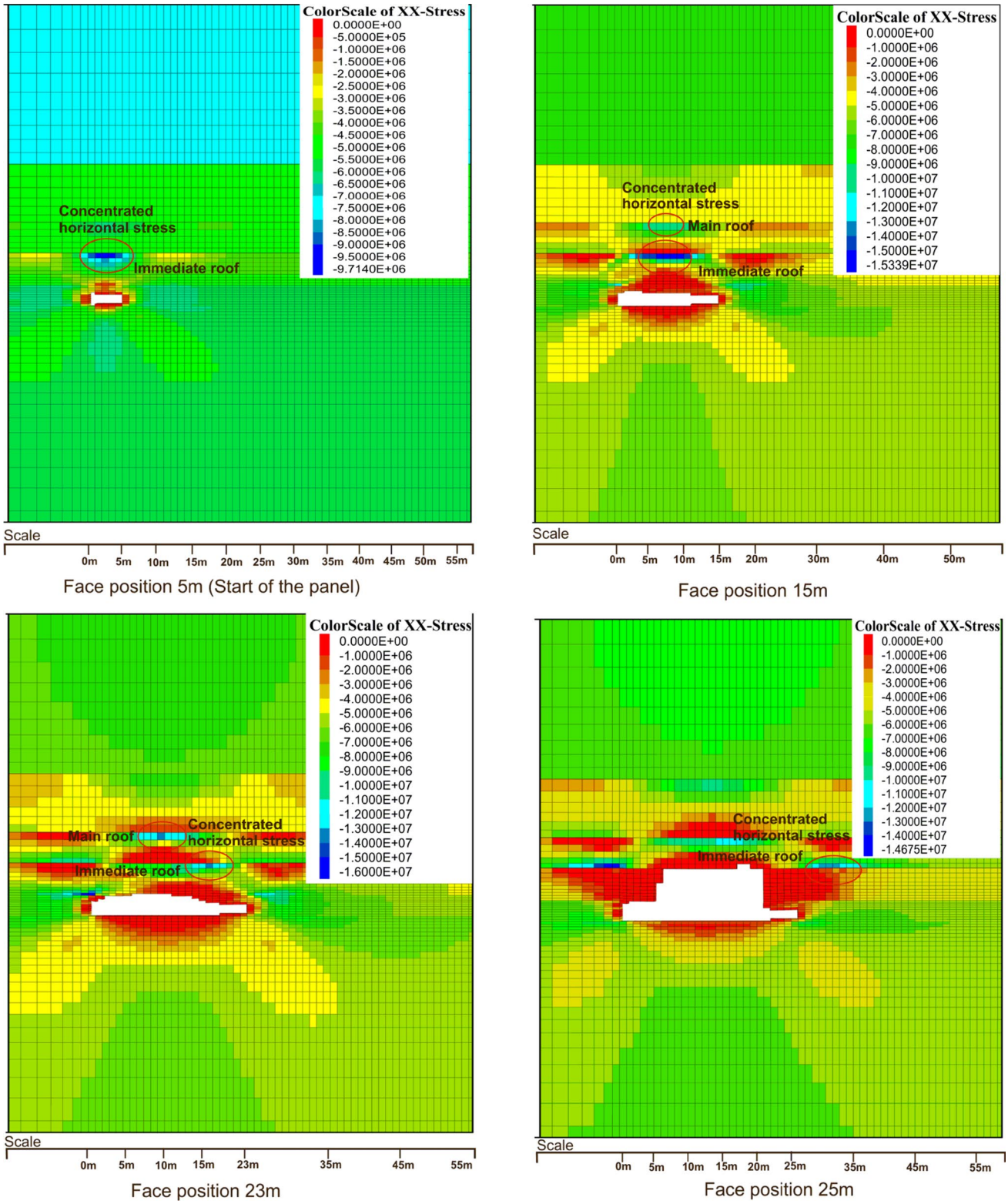

Fig. 9 Concentration of horizontal stress in overlying strata of Working 'A'

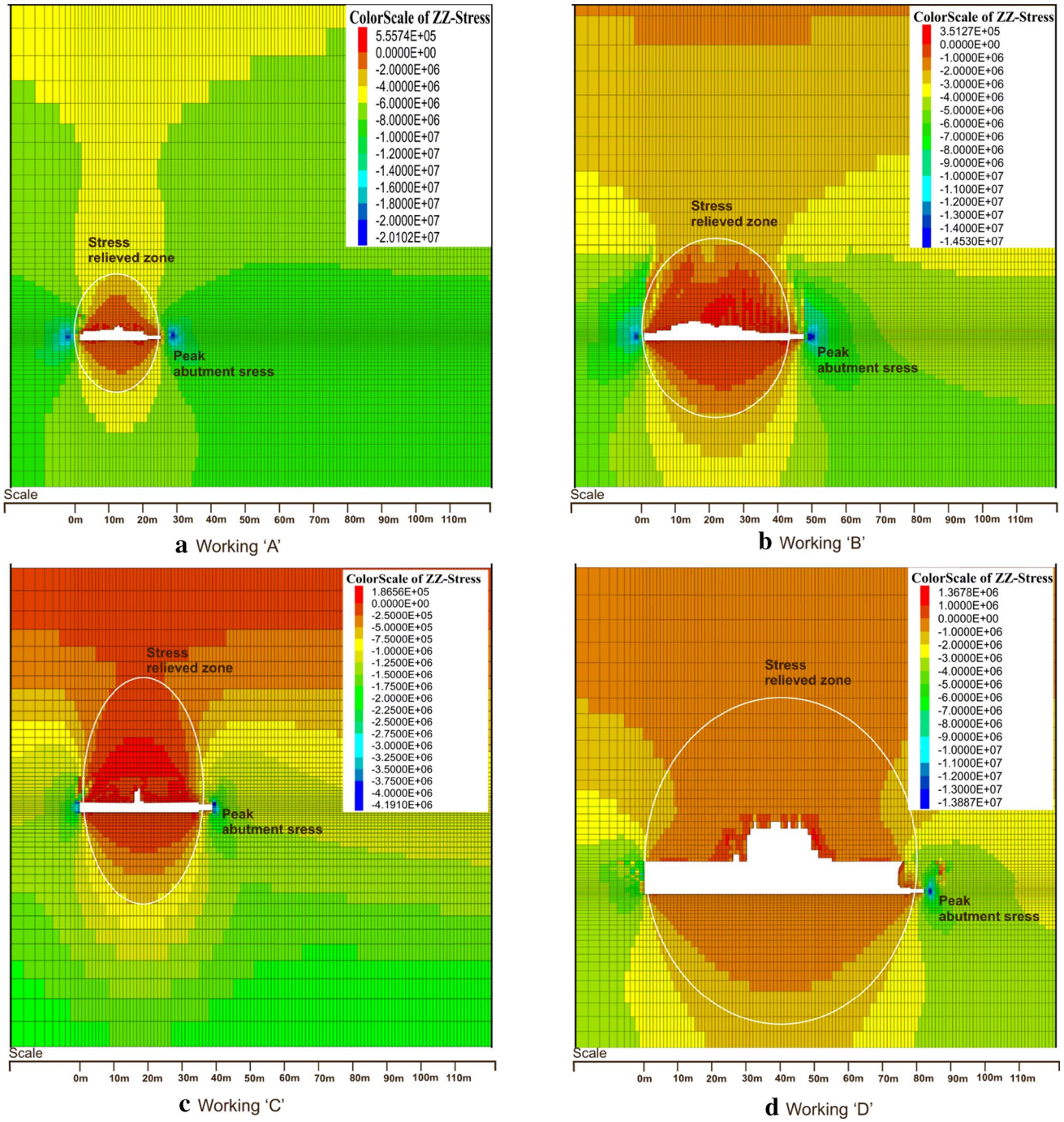

Fig. 10 Distribution of stresses at peak abutment for Workings 'A', 'B', 'C', and 'D'

5.2 Failure and Caving of Strata

Figure 12 shows the state of failure in overlying strata before caving of the main roof in the four different workings. In general, the failure of the rock material was distributed upward in the roof and downward on the floor and in some cases ahead of the face. In Workings 'A' and 'B', the dominant mechanism of failure was shear, whereas the tensile mode of failure was dominant in Workings 'C' and 'D'. The first caving of the immediate roof just above the face was experienced at 12 m face advance in Working 'A' and 40 m face advance in Working 'B'. Similarly, in Workings 'C' and 'D', the first caving was realized at the face advance of 39 m and 56 m, respectively. The competency of the strata, shallow depth of working, and formation of large overhang behind the face were the prime reasons for the

Table 2 Ratio between the heights of stress relieved zones to the face advance in four workings

	The height of stress relieved zones (h_{st}), m	Face advance (f_a), m	h_{st}/f_a ratio
Working 'A'	20	24	0.83
Working 'B'	31	48	0.64
Working 'C'	18	39	0.46
Working 'D'	42	82	0.51

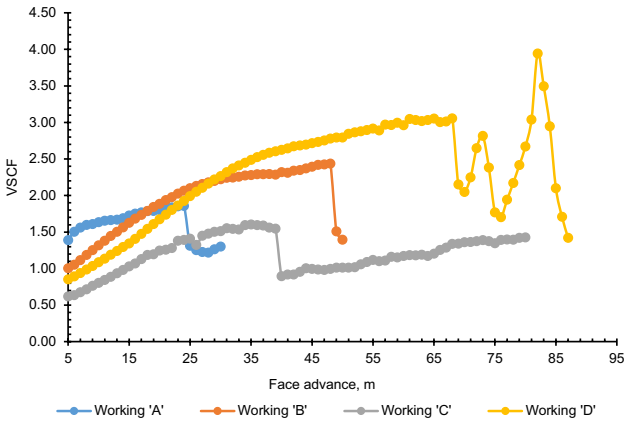

Fig. 11 Vertical stress concentration of four workings with progressive face advance

delayed caving in Working 'D', while the thick immediate roof was the major cause of such observation in Working 'B'. The subsequent caving of immediate roof was observed at every 4–6 m interval of face advance in Workings 'A' and 'D' while regular caving of immediate roof was observed at every 1–2 m of face advance in Workings 'B' and 'C' owing to relatively softer nature of the strata.

In Working 'A', the process of rupture initiation in the main roof started after 18 m of face advance, which moved gradually upward to the upper layer with progressive mining. The main fall was observed at face advance of 25 m when 5.8 m-thick roof caved behind the face with the peak load of 325 t on the face support. In the field, as well, the failure of the main roof was observed at the same stage of face advance with yielding of the face supports. In Working 'B', the event of caving en masse was experienced due to the presence of a thick immediate roof of 30 m, which caved after 49 m of face advance along with caving of the main roof. As a result, a total 42 m-thick roof participated in the en masse caving, causing a serious loading condition at the face. In the field, a total of 62 leg circuits were noticed in the yielding state in response to this heavy weighting event. The affected zone of the face was from chock No. 20 to 80, covering 60% of the face length with maximum impact at its center.

In Working 'C', the failure process of the main roof initiated at 70–72 m face advance (Figs. 12c, 15, 16c). The average load on the support during this period was recorded as 446 t. In the field, a similar observation was noted at face advance of 67 m without any deformation of the overlying roofs. The ultimate caving of the main roof was observed at face advance of 89 m in the model, while the field-observed caving span was 81 m, which was also accompanied by yielding of 163 hydraulic leg circuits. The modeling results showed that nearly 24.5 m-thick main roof caved during the main fall, which ultimately triggered the yielding of a large number of hydraulic leg circuits. The field observations showed 50–450 mm of support closure in chocks 20–40, with an average of 150 mm during the main fall.

In Working 'D', the tensile failure of the main roof initiated at the center of the beam and progressed upward at 68 m of face advance (Fig. 12d). In the first phase, 5.32 m-thick portion of the main roof failed in tension and gradually progressed upward with further mining. When the face advanced to 70 m, the load on the support was raised to yield load of 550 t, while the main roof spanning over 32 m underwent failure up to 6 m in the vertically upward direction. The failure process of the main roof was dominated by tensile failure. The ultimate caving of the main roof was observed at 87 m face advance when 15.45 m-thick roof caved behind the face over 68 m of span in the direction of mining. Starting from the initiation of failure to the ultimate caving, the face witnessed a series of weightings at every 5–10 m interval of mining due to the staged failure of the thick hard roof. The entire process of caving was controlled by the strata properties, particularly the thickness of the main roof, its deformation modulus, and their location above the coal seam, as also agreed by Shabanimashcool et al. (2014).

Figure 13 plots the normalized value of the bending stress (ratio of the induced value of σ_{xx} to the in situ horizontal stress) with the progressive advance of the face in four workings. The maximum stress was often concentrated in the upper portion of the main roof before its ultimate failure and caving in all the four workings. Furthermore, the maximum bending stress was realized in the Working 'D' followed by the Workings 'A', 'C', and 'B'. This was mainly due to the presence of a thick sandstone roof with high elastic modulus and compressive strength in the working. As a consequence, a series of weighting in every 5–10 m interval was realized before the ultimate caving of the main roof at 87 m in this case. In Working 'A', the span of maximum bending stress was realized after 13 m of face advance, whereas the span was realized just before caving of the main roof in Working 'C' and 'B'. Higher depth of working with the high-stress environment and laminated rock formations were the major reasons that resulted in maximum bending stress at a lower span in the Working 'A'.

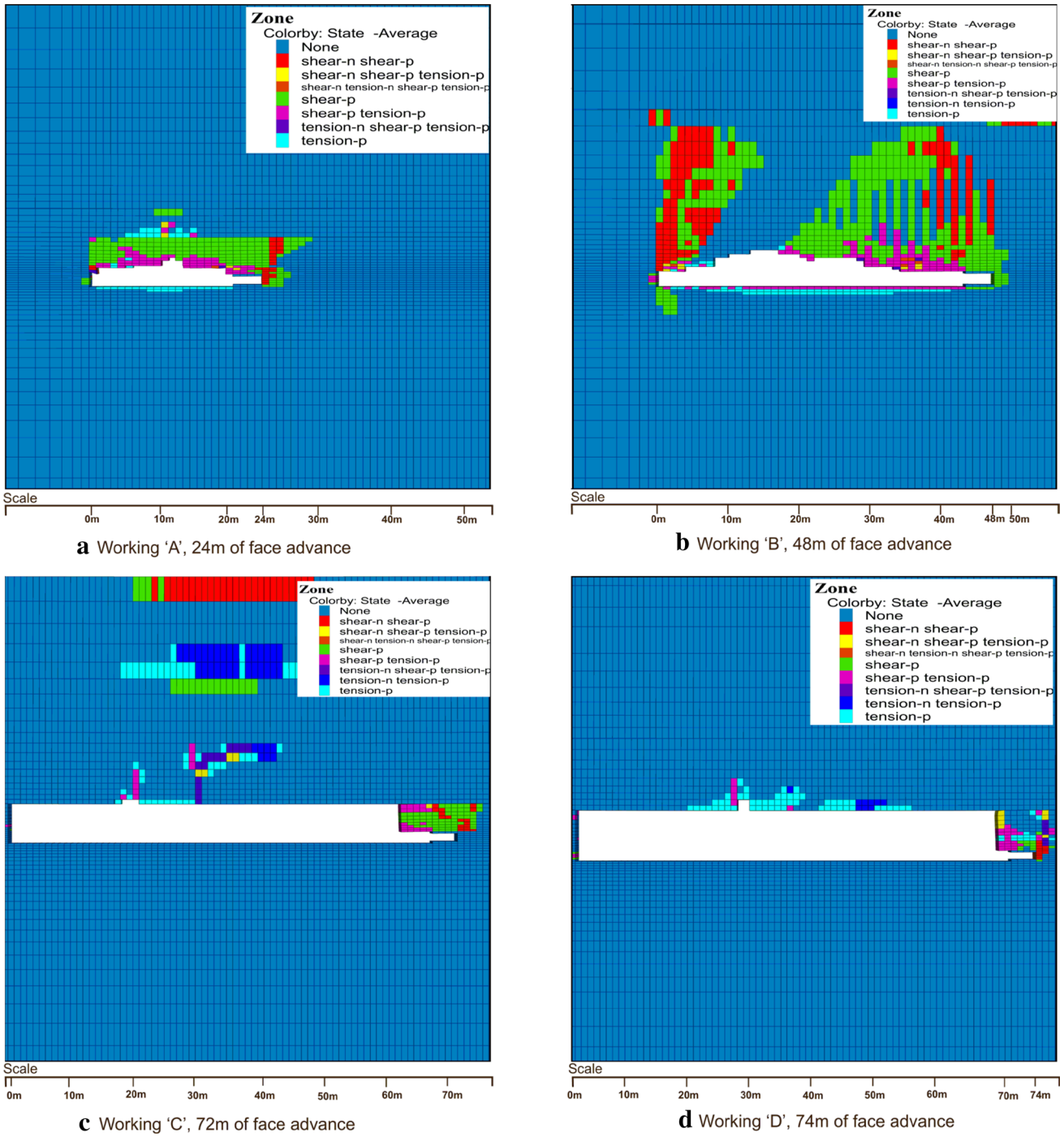

Fig. 12 Failure state of material during rupture of the main roof

Figure 14 plots the caving angle during the initial stage and the final stage of caving, as observed during the main fall in the four workings. The first instance of caving was observed after 24 m face advance in Working 'A' with a caving angle of 16°, which involved 2 m thick and 3 m lateral length of the main roof. The ultimate caving angle in Working 'A' was 90° at the time of the main fall, observed at face position of 25 m. During this period, the support load of 325 t was experienced at the center of the face. Similarly, the first caving of the main roof in Working 'B' involved a 9 m-thick roof covering 31 m lateral distance with caving angle of 40°. The load on the support during this event was 676 t. At face position of 49 m, the main roof caved completely with caving angle of 74°. The initial and ultimate caving angles

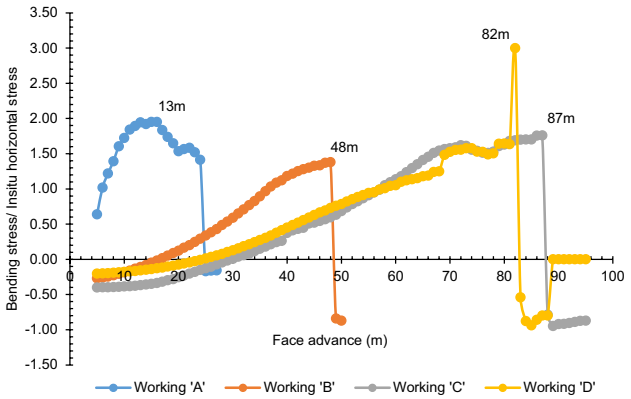

Fig. 13 Bending stress concentration in the main roof versus longwall face advance in four workings

during the first and ultimate caving of the main roof were 34° and 44° in Working 'C' and 24° and 62° in Working 'D', respectively. In Working 'C', the supports were observed in yielding conditions starting from the initial stage to the final stage of main fall, whereas the load on the support reached 90% of the yield load during the initial caving of the main roof in Working 'D'.

5.3 Progressive Face Convergence and Cyclic Loading of Roof Support

During the simulation of progressive mining cycles, face convergence and the load on the supports were monitored to understand the deformation (Fig. 15) and loading characteristics of the overlying strata near the face (Fig. 16a–d). From the modeling results, it was noticed that the values of peak convergence slope near the working face for the four Workings 'A', 'B', 'C', and 'D' were 4, 21, 8, and 10 mm/m, respectively. The peak convergence was observed due to the lowering of the main roof during the main fall. The convergence slope was marginal in the initial phase of face advance, but the value suddenly increased to its peak in all the four workings once the face reached the weighting period. Although the longwall face in Working 'A' was operated at greater depth, the average convergence experienced was minimum due to the regular caving of the laminated strata. In contrast, due to the presence of thick immediate and main roofs, the peak convergence was at the higher side resulting in caving en masse during the main fall in Working 'B'. In Workings 'C' and 'D', the convergence slope gradually increased due to the formation of large overhang behind the face and reached the maximum value before the main fall and got relaxed afterward.

The load on the support with progressive mining in all the four workings is plotted in Fig. 16. In Working 'A', the first instance of significant load on the support was observed at the face advance of 10 m with the support load of 242 t. The support load slightly increased to 255 t at the time of the first local fall, while its value was 245 t during subsequent local fall. The first instance of peak load was experienced during the main fall at 25 m face advance. The weighting lasted for only three mining cycles when the support achieved a peak load of 325 t and got relaxed thereafter due to the ultimate caving of the main roof.

In Working 'B', the rise in support load with progressive mining followed a linear trend due to the formation of the large overhang of thick immediate as well as main roofs. With progressive advancement of the face, the load on the support gradually built to 676 t till face advance of 48 m. The first instance of peak load up to the yield load of 760 t was observed at the face position of 49 m due to the caving en masse of the immediate as well as the main roof.

In Working 'C', the face was operated at 50 m cover depth with a support capacity of 450 t. Under this condition, the overlying strata remained hanging up to 30 m of face advance without any significant loading of the support. A support load of 375 t was experienced at face position of 34 m due to the deformation of the failed immediate roof and reached to 432 t before the first instance of the immediate roof caving that led to local fall. During face advance from 45 to 70 m, the load on support increased gradually from 414 to 436 t. At face position of 72 m, the support load of 447 t was experienced due to the initiation of failure in the main roof. The support load reached its peak value for the first time at face position of 80 m, where the failed portion of the main roof started to deform, leading to the main fall. The weighting period lasted up to ten mining cycles till 89 m of face advance, and the support load decreased after the ultimate caving of the main roof.

In working 'D', the support load of 434 t gradually developed with progressive mining till 69 m of face advance. It achieved a yield load of 550 t at 70 m face advance when the first weighting at the face was observed. The face experienced a strong weighting event before caving of the main roof at 87 m face advance. It was mainly because of the presence of 16 m strong bed, which failed and deformed gradually during 70–87 m of face advance (Fig. 16d).

An overall analysis of the loading pattern experienced by the supports deployed at the face showed that in Working 'A', the loading of the support was almost constant until the main fall occurs. The load on the support at the end of a mining cycle increased by 13–25% of its setting load. However, the support load experienced a continuous built-up until it achieved the yield load in Workings 'B', 'C', and 'D'. The support deployed in Working 'D' experienced the least incremental loading, whereas the support deployed in Working 'C' had the maximum rate of load increment. These observations of cyclic loading patterns during progressive mining indicated that the support of 4×450 t capacity

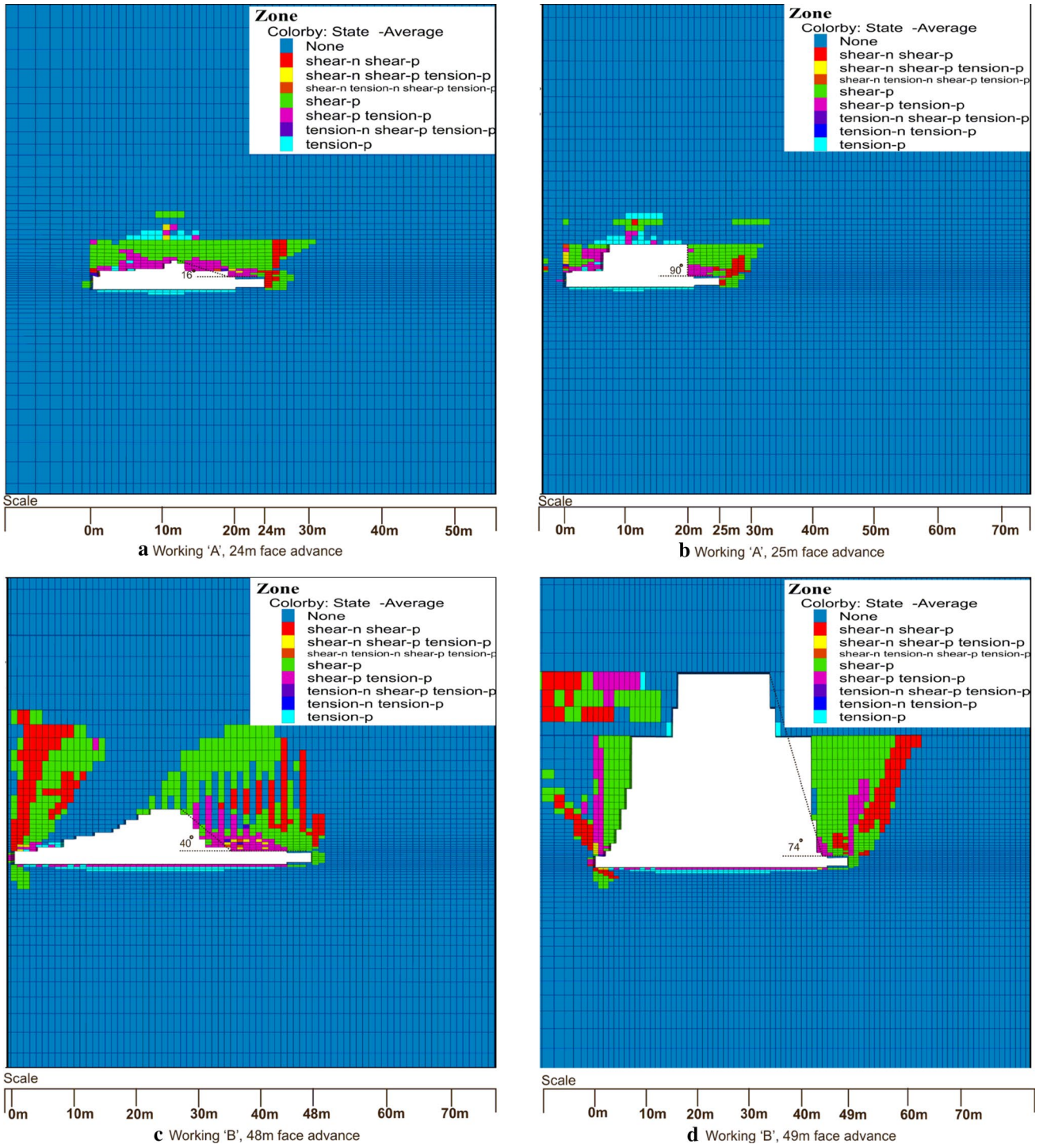

Fig. 14 Caving angle during the initial and the final stage of caving of the main roof in the four workings

deployed in Working 'C' was under-rated as it suffered extreme loading conditions in most of the mining cycles, as also confirmed through field experiences. These observations of cyclic loading of face support also validate the findings reported by Medhurst and Reed (2005) and Trueman et al. (2009).

5.4 Face Instability

The observation of failure state and horizontal movement of the coal face during the main fall at all the four study sites is shown in Fig. 17. In Working 'A', the extent of the failed zone was observed up to 4 m ahead of the face. Most of the

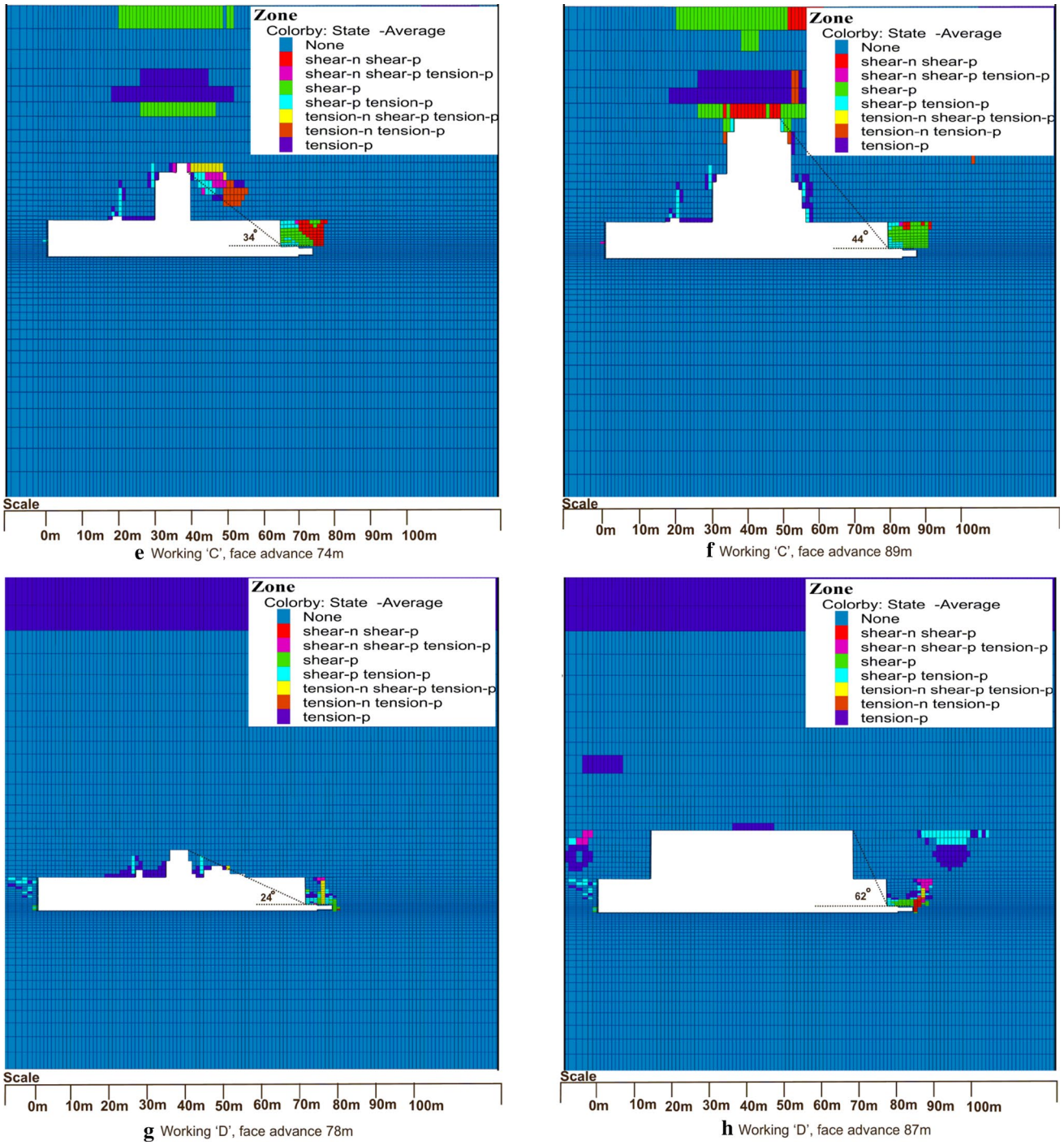

Fig. 14 (continued)

zones at the coal face yielded in shear mode (Fig. 17a). The failed zones were distributed from the top to the bottom of the face. The top corner of the face experienced the maximum horizontal displacement of 72 mm during the period of the main fall. In Working 'B', the extent of the failed zone was observed up to 2 m ahead of the face. All such zones were failed in shear. The formation of the yielded zone first started at the center of the face and propagated gradually upward as well as downward with progressive face movement. The maximum horizontal displacement of 24 mm was observed at the center of the face. Interestingly, no zone was found in yielding conditions until the main fall in Working 'C'. The maximum horizontal displacement of 10 mm was observed at the top corner of the longwall face. Such

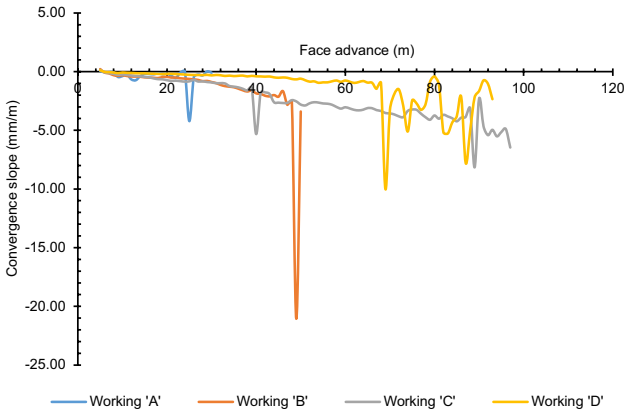

Fig. 15 Average convergence slope at working face with progressive mining

observations were primarily related to the nature and the loading condition of the strata. The depth of the mine was also one of the main factors for such typical observations. In Working 'D', a 3 m-thick zone ahead of the longwall face underwent failure starting from the face corner to the face bottom. All the zones failed in shear. The maximum horizontal displacement of 12–15 mm was observed at the face corner. On closer scrutiny, it was observed that the failure process of the coal face depended on the elastic properties of the coal seam, of the roof, and the floor of the workings. In all the four workings, the failure of the coal face initiated from the center of the face and progressed gradually upward or downward depending on the stiffness of the overlying or underlying strata.

Y-axis: Support load, MN
X-axis: Solution steps

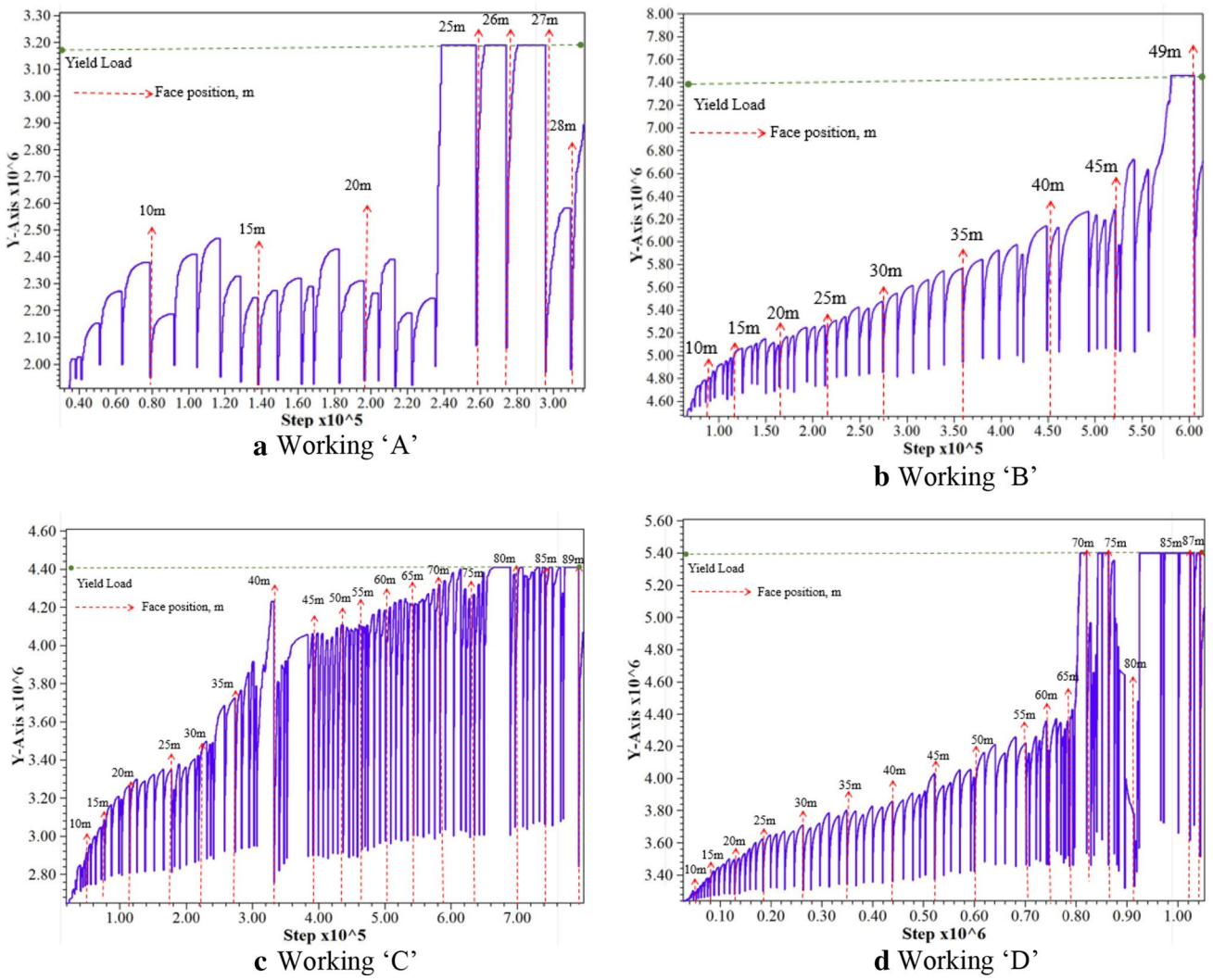

a Working 'A'

b Working 'B'

c Working 'C'

d Working 'D'

Fig. 16 Cyclic loading of the support till main fall in the Workings, 'A', 'B', 'C', and 'D'

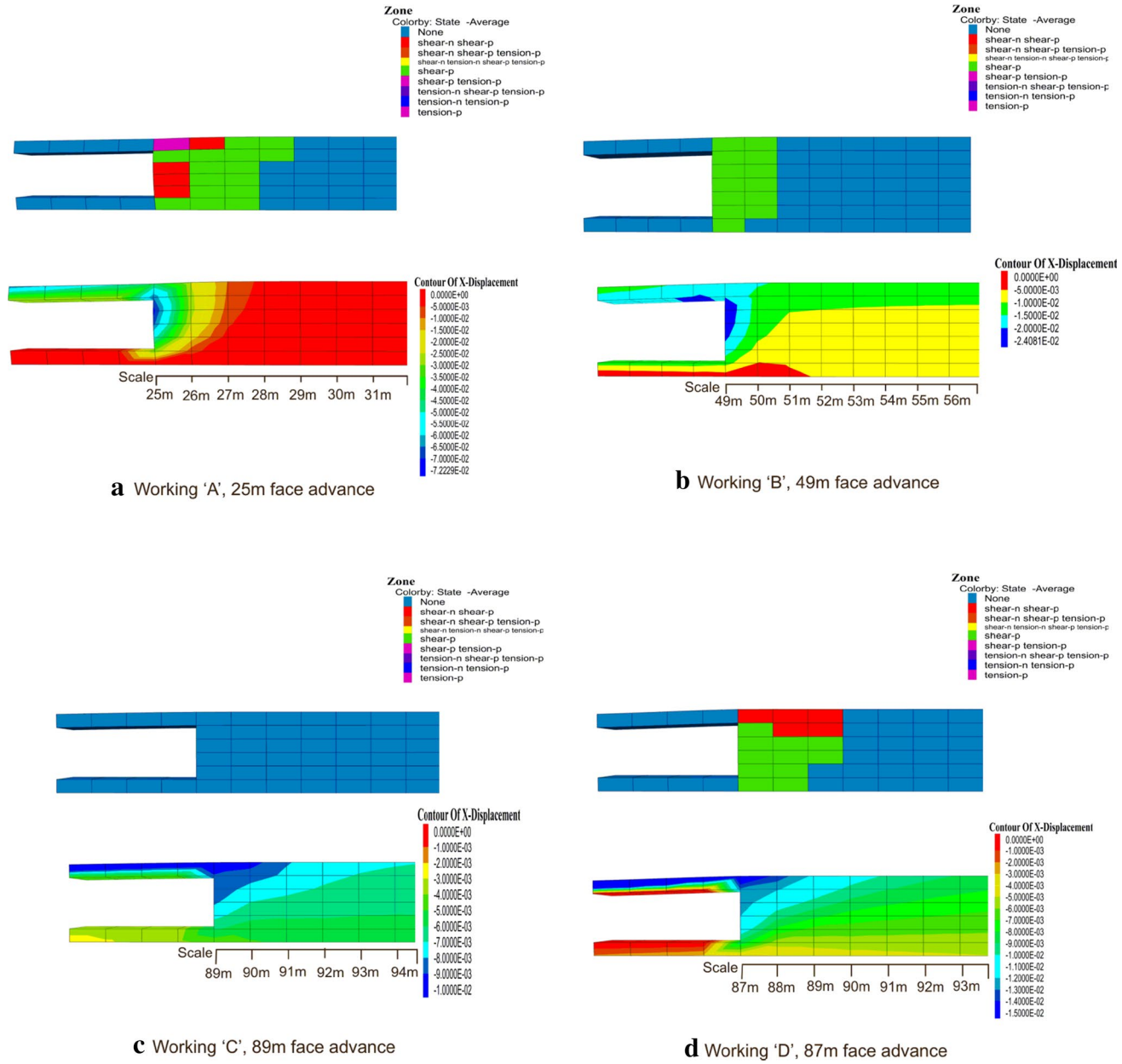

Fig. 17 Extension of the failed zones and horizontal displacements at the center of the longwall face during the main weighting

To investigate the relationship between the stress and strain parameters during failure, Fig. 18 plots the relationship between the axial strain and the vertical and horizontal stresses during peak stress period at the four longwall faces. It can be observed that in Working 'A', the vertical stress reached its peak value of 19.4 MPa at the distance of 4 m ahead of the face and then continuously decreased beyond this region. On the contrary, the horizontal confining stress reached its peak value of 8.7 MPa at the distance of 6 m ahead of the coal wall and then decreased to 0.6 MPa at the monitoring point of the coal wall which resulted in a 96% reduction in confinement from the peak observed value. The distribution of axial strain confirmed that the face was axially strained by 2.5% at the face, and the axial strain continuously decreased away from the face. Based on the field and the model observations of face failure within 4 m region ahead of the face, 0.5% of axial strain could be taken as the threshold limit beyond which the face got destabilized. As the confining stress decreased due to the failure of the coal wall, the concentration of peak abutment stress penetrated deeper into the coal wall till the end of the failure regime. A similar mechanism was observed in Workings 'B' and 'D' as well. The depth of the failure region in Workings 'A', 'B', and 'D' is shown

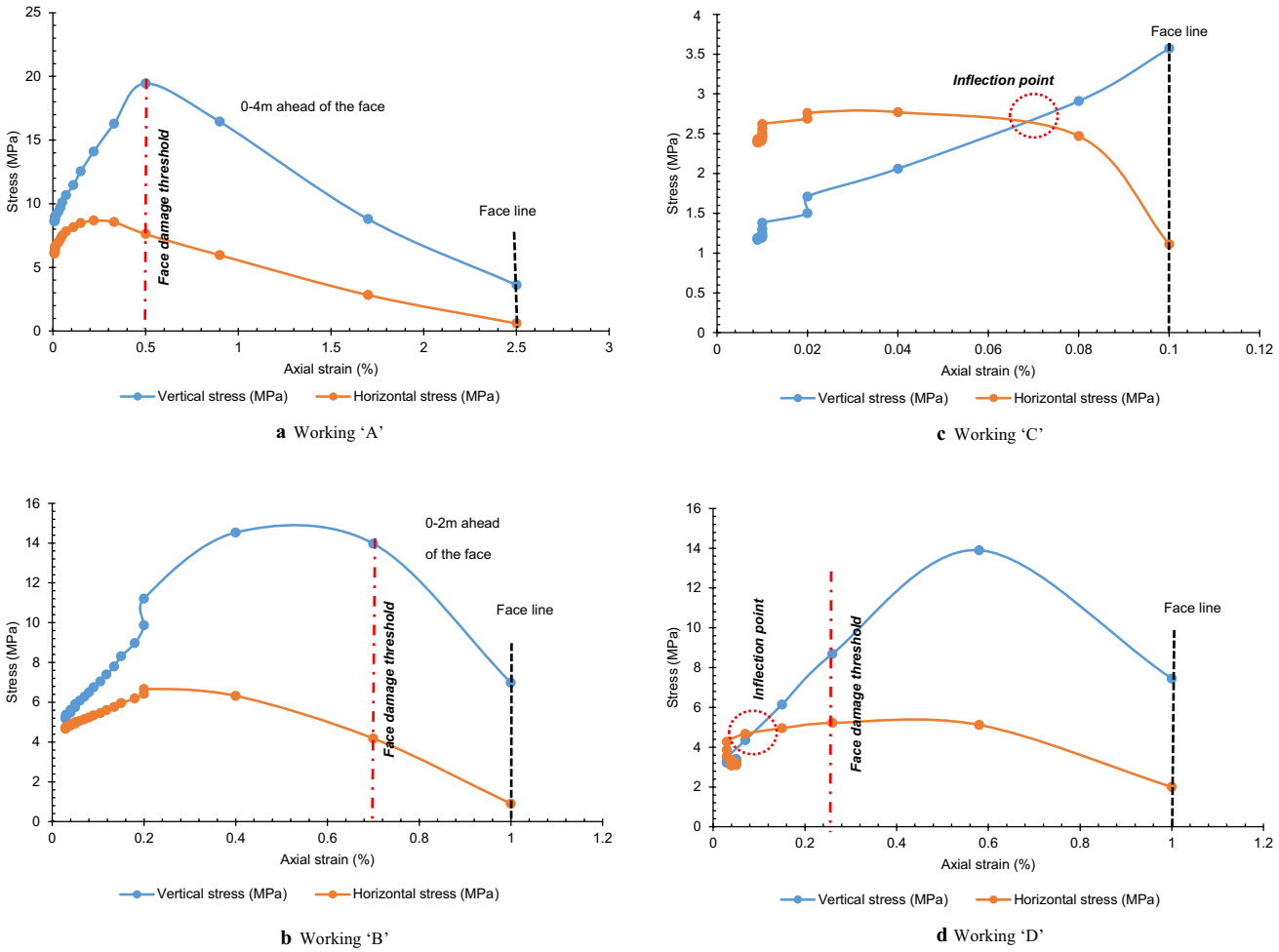

Fig. 18 Stress–strain relationship at the longwall face during peak stress period in four workings

in Fig. 18. The threshold limit of axial strain in Workings 'B' and 'D' was 0.7% and 0.26%, considering the field and model-based observations of the depth of failure and interaction of vertical and horizontal stress paths at the coal wall. The stress paths realized around the coal wall of Working 'C' suggested that the vertical and the horizontal stress trajectories intersected each other 2 m ahead of the face due to the increase in confining stress, which superseded the vertical stress beyond this region. The intersection point of stress path in Working 'C' could be considered as the point of inflection beyond which the face gets stable due to the increase in confining stresses against the induced vertical stresses ahead of this point. From the field observations, it was also established that beyond 2 m ahead of the face, the rock behaved elastically, and no such failure was found at the coal wall during strata weighting. In Working 'D', the point of inflection was found 5 m ahead of the face, which indicated plastic damage of the face within this region with failure depth of 3 m as a result of the weighting.

6 Discussion

An in-depth study was carried out to understand the geo-mechanical response of the strata under varying geo-mining conditions represented by four different longwall workings belonging to different coalfields in India. The finite-difference modeling approach was applied to study the pattern of stresses redistribution, mechanism of strata failure and caving, progressive face convergence apart from cyclic loading of the support, and face instability mechanism till the completion of main fall in the selected workings. It was found that the magnitude, direction, and concentration of principal stresses largely depend on the mining depth and elastic properties of the overlying strata. At shallow depth workings (Workings 'C' and 'D'), the major principal stress was often concentrated in the roof and floor of the working, whereas the concentration of stresses was noticed ahead of the coal face in high-to-moderate depth workings (Workings 'A' and 'B').

The concentration of peak abutment stress was observed 2–5 m ahead of the face in all the four workings depending on the length of overhang formed in the goaf. The formation of overhang in such workings was primarily controlled by the strength properties and thickness of the overlying strata along with their bending behavior at different depths of working. In Working 'A', the concentration of abutment stress was realized at 4–5 m ahead of the face due to the effect of the high working depth, whereas higher values of the peak VSCF were noticed in Workings 'B' and 'D' owing to the formation of large overhang under the thick and strong roof layers. The nature of overhang formation is also important in deciding the amount of stress relieved zone in the goaf, which contributes to high volume caving and impact loading of the support and the face. The events of en masse caving and dynamic support loading at longwall faces in Workings 'B' and 'D' were the by-products of such a mechanism. In all the workings, the concentration of vertical stress is gradually increased and reached the maximum value just before the failure of the main roof.

The type of formations (laminated or massive) along with the strength properties of various rock layers within the caving zone is crucial in defining the nature of caving (regular/delayed) in longwall operations. As discussed, nearly 50–85% of Indian coal measure rocks are comprised of sandstone in the zone of caving in such operations. Irrespective of the rock type, the laminated strata formations cave easily after the advancement of the support without forming any significant overhang in the goaf, as observed in Working 'A'. In contrast, thick and strong formations form a large overhang and cause dynamic loading to the support during the failure and subsequent caving of the strata, as observed in the remaining three Workings, 'B', 'C', and 'D'. In Working 'A', the large amount of induced stress that developed because of deep mining condition resulted in the shear failure of strong but laminated sandstone layers. The impact of such strata failure and caving was insignificant due to the regular caving of the strata. Although the strength of the roof layers was relatively high, the laminations present in the strata enabled them to cave at regular intervals with the progressive face advance. On the contrary, although the roof strata of Working 'B' were weaker, the high thickness of such roof resulted in the formation of 47 m long overhang which ultimately triggered en masse caving in the goaf followed by yielding of a large number of hydraulic legs as observed in the field. In Workings 'C' and 'D', which were representative of shallow depth working, thickness and mechanical strength of the main roof often control the intensity of its failure and caving. The presence of thick and strong main roof caused delayed caving of the main roof and a series of yielding event of powered supports deployed in such conditions. The tensile mode of failure dominated the overall failure process in such operations. Irrespective of the above conditions, the caving of the immediate roof is not considered as the potential threat to strata control unless it is very thick.

The role of bending stress in separation and caving of the main roof is critical in terms of the nature of caving and loading on the powered support. The magnitude of the induced bending stress mainly depends on the elastic properties and thickness of the participating roof. The more the elastic modulus and the thickness of the roof, the higher is the induction of bending stress, which ultimately helps in forming a larger overhang causing a delay in caving and impact loading on the supports. The strata control observations at Working 'D' perceived similar experience where the bending stress was found in order of three times the in situ horizontal stress.

Estimation of caving angle and length of the overhang of the main roof helps in determining the nature and volume of rock involved in the process of caving. The lower angle of caving with the formation of large overhang signifies delayed caving, whereas the larger angle of caving with a shorter span of overhang confirms an easy caving condition, but caving en masse involves a large volume of rock undergoing failure over a very small interval of face advance. It was found that the magnitude of the caving angle depends on the nature of the formation, thickness, and elastic properties of the strata and the depth of the mining. If the strata are competent enough, the caving angle is often relatively low, while the larger angle of caving is expected during the major caving in case of soft strata. In Working 'A', the laminated strata under high working depth caved with caving angle of about 90°, while the thick and competent strata in Working 'C' caved with caving angle of 44° under the shallow depth of working. As the overlying strata of Working 'A' caved with maximum caving angle, the loading lasted for only one mining cycle during the main fall in the absence of large overhang. In comparison, at Working 'C', the formation of large overhang with a lower caving angle caused significant loading on the support during the period of major caving. These observations show that the initial angle and the final angle of caving of the main roof and the extent of face advance in-between are essential for deciding the associated irregularity of caving of the strata and the severity of resultant loading of the face support.

The model findings of the four sites showed that the rate of face convergence varied with the competency of the strata and the depth of mining. The movement pattern of the main roof and resultant roof convergence are the key factors that control the severity of roof deformation and loading of roof supports during the progressive advance of the face. If the strata formation is laminated, the rate of convergence is relatively low. Therefore, in Working 'A', although the face was operated at large depth, the laminated nature of strata resulted in a relatively low rate of face convergence.

However, the presence of massive immediate roof and large overhang resulted in mounting the convergence rate till caving of the main roof strata in Working 'B'. The rate of rising in face convergence was maximum in Working 'C' among all the four workings due to mining in shallow depth and influence of thick sandstone roof, which eventually caved after 89 m of face advance. In Working 'D', the staged failure of the main roof led to the periodical rise in face convergence at every 5–10 m of mining interval. The maximum rate of convergence in Workings 'A', 'B', 'C', and 'D' was identified as 4, 21, 8, and 10 mm/m, respectively. The maximum convergence rate at Working 'B' indicated a heavy weighting event, which is in good agreement with the field observation of en masse caving in that working.

Based on the field and model observations, it was also observed that the capacity of powered supports deployed at the Workings 'A', 'B', and 'D' was technically suited to the respective geological environment. It was experienced that due considerations need to be given to the nature, thickness, and physicomechanical properties of the rock layers present in the caving zone while selecting the capacity of powered support. The performance of face support was least affected due to the regular caving of laminated formation of strata in Working 'A'. However, the presence of thick and strong sandstone roof requires due attention for optimum selection of powered support through scientific assessment of rock characteristics and their breaking strength. Similarly, if the immediate composite layer is thick as prevailing in the Working 'B', it was evident at many occasions that the roof caved right from the face along with the main roof which transferred a significant load of the massive roof to the shield support during periods of major roof caving. In such circumstances, the heavy weighting events affect operating cycles of powered support, causing critical damage to the face infrastructures in extreme cases. The stability of the coalface also gets affected in response to these weighting events. Rational selection of powered support capacity considering the behavior of the strata is crucial to avert potential damage in such workings.

The support load-time steps' chart of Working 'C' indicated that the shield was overloaded, and the rate of loading did not reduce until the main fall occurs. Based on the analysis of rock–strata interaction at Working 'C', it was confirmed that the selected support was not enough to control the energy transferred by the deflection of 24.6 m-thick sandstone roof, which was located 5.5 m above the mining height. The selection of under-rated capacity of face support was the prime reason for such observation in Working 'C'. In Working 'D', the main roof underwent failure in stages after 68 m of face advance at every 5–10 m interval of mining. As a result, a series of weighting events were experienced before the ultimate failure of the main roof at 87 m face position. The face convergence observation also compliments the same phenomenon at Working 'D'. In the presence of a thick sandstone roof in the immediate vicinity, the shield supports got periodically or continuously loaded as observed in Workings 'C' and 'D', depending on the rated capacity of the support deployed in such conditions. Under such circumstances, ensuring the consistent setting load is extremely difficult in the presence of a weak immediate roof while continuous overloading of the support may trigger the cavity formation in the roof, resulting in a prolonged delay in face progress. No such events were encountered in Workings 'C' and 'D' due to the presence of a strong immediate roof above the mining height.

The observations of face failure at the four workings suggested that the face instability mechanism was dominated by shear failure in the majority of the cases. The process of coal wall yielding was governed by the loading environment, coal strength, and state of stress around the longwall face. It was observed that the ultimate strength and the confining stress in the coal wall gradually decreased with progressive mining, and the failure occurred when the peak vertical stress surpassed the ultimate strength of the coal wall. From the start of the mining, the increasing abutment stress and decreasing confinement weakened the coal wall, which led to its failure in shear. However, the depth of the coal wall failure depended on the working depth, coal mass strength, as well as the location of peak abutment stress ahead of the face. Out of the four workings, the coal wall of Working 'C' remained stable even in the period of weighting due to the higher coal strength and shallow depth of mining. On the contrary, the coal wall of Working 'A' experienced failure to the maximum depth of 4 m ahead of the face owing to the lower rock mass strength and concentration of high vertical stress associated with the greater depth of working. The maximum horizontal displacement of 72 mm in the coal wall was observed in Working 'A' during the period of the main fall. Additionally, it was also found that the pattern of face failure was mostly controlled by the ratio of elastic modulus of the immediate roof and floor to that of the coal wall as the required confinement was provided by the section with a higher modulus. In all the workings, the failure process and horizontal movement of coal face were initiated from the center of the face, and progressed gradually upward or downward depending on the softness of the roof or floor strata, respectively.

The observations of vertical and horizontal stresses and the axial strain relationship during the peak stress period suggested that the structural integrity of the coal wall was destabilized when it crossed the threshold value of the axial strain of the respective working. The threshold value of axial strain for Workings 'A', 'B', and 'D' was identified as 0.5%, 0.7%, and 0.26%, respectively. Interestingly, the stress trajectories of Workings 'C' and 'D' intersected each other beyond 2 m and 5 m ahead of the face, which indicates that

Table 3 Comparisons of some of the critical geo-mechanics in Indian longwall operations

Geo-mechanical characteristics	Present model results	Observations of various researchers	References	Field observations	Remarks
Location of peak vertical stress concentration ahead of the face	2–5 m	2–4 m	Singh and Singh (2009) Islavath et al. (2016)	1-3 m	The stress concentration observations at the field may vary with the model results as the local discontinuities have not been considered in the current model
Caving angle	44°–90°	27°–90°	Das (2000)	–	–
The ratio between total affected roof height and mining height	Five to 15 times the extracted thickness	Four to 8.5 times the extracted thickness	Das (2000)	Four to 15 times the extracted thickness	–
The ratio between immediate caving height and mining height	Two-to-four times the extracted thickness	Two-to-six times the extracted thickness	Das (2000)	Two-to-six times the extracted thickness	–
Cavability class of four workings based on caving characteristics and caving angle	Working 'A' Extremely cavable Working 'B' Very good cavable Working 'C' Poor cavable Working 'D' Good cavable	Working 'A' Extreamly cavable Working 'B' Good cavable Working 'C' Poor cavable Working 'D' Good cavable	Das (2000)	Working 'A' Extremely cavable Working 'B' Very good cavable Working 'C' Poor cavable Working 'D' Good cavable	–
Depth of failure of the coal face	1–4 m	1–2 m	Islavath et al. (2016)	1–3 m	The field observations may vary with the model results as local discontinuities have not been considered in the current model

beyond this point, the face would behave elastically due to the increase in confining stress as compared to the vertical stress in the respective cases. The point of inflection acts as an isolator between the plastic and elastic regions ahead of the coal face.

The broader findings of the present study are validated in terms of the caving span and the support loading pattern perceived during field operation at the selected sites of the study. Some of the critical geo-mechanics as perceived in the model are also compared with the pertinent observations reported by some other workers, as shown in Table 3. The results of the current approach are in good agreement with the overall characteristics of longwall geo-mechanics reported by several researchers in varying mining conditions (Medhurst and Reed 2005; Peng 2006; Trueman et al. 2009; Singh and Singh 2010a, b; Qian et al. 2010; Shabanimashcool et al. 2014; Bai et al. 2016; Prusek et al. 2016; Verma et al. 2016; Kang et al. 2018; Mohammadi et al. 2018; Wang et al. 2018; Kong et al. 2019; Liu et al. 2019). Hence, the confidence gained from this exercise demonstrates that the present numerical modeling approach can be safely used in the planning and design of longwall workings.

7 Conclusion

The underperformance of longwall workings in India may be attributed to inadequate geological and geotechnical characterizations, improper designs of panels, and selection of under-rated support capacities. These lacunae in characterization and design negatively influenced the safety and productivity of various projects. This study attempted to bridge this gap through numerical analysis of the longwall faces pertaining to four coalfields namely JCF, RCF, S_tCF, and GCF, under variable mining depths. The results of the models were verified against the available field data and previously published literature. The study confirms that the mechanical properties of the overlying strata and the depth of workings were the major controlling parameters for defining the strata behavior in longwall workings. The major conclusions drawn from this work are as follows:

- The properties of strata, mining depth, and the length of overhang in the goaf contribute to the concentration and location of peak abutment stresses ahead of the face.
- At greater depths, the dominant mode of failure is shear, but the tensile mode of failure is dominant at the shallow depth workings.
- The instance of large overhang formation and the maximum value of peak vertical stress concentration factor (VSCF) was recorded in Working 'D' due to its shallow depth of cover and the high strength properties of the strata.
- In Working 'C', even at shallow depth, the observed stress concentration was relatively low due to the soft nature of the strata.
- Among the four sites, the highest value of VSCF (3.94 times the in situ stress) was recorded in Working 'D', whereas the lowest value was recorded in Working 'A'.
- Owing to the greater depth of cover, the caving of strata in Workings 'A' and 'B' occurs at a lower span causing low-stress concentration at the face in these conditions.
- The observation of peak abutment stress concentration that occurred 2–5 m ahead of the face in all the four workings corroborates the field observation for the Indian longwall panels.
- The investigation revealed that the formation of strata, its mechanical strength, and the depth of mining were crucial in defining the caving behavior under Indian geological formations.
- The main fall span of Working 'C' was observed after 89 m face advance because of the presence of thick and competent main roof and shallow depth of cover. The caving of the main roof in the Working 'A' was found after 25 m of face advance due to the laminated strata formation and high depth of cover.
- The findings of bending stress concentration in the main roof indicate that the elastic properties and the thickness of the main roof are critical in terms of concentration of such stresses apart from the formation of overhang, nature of caving, and impact loading on the support.
- The initial and final caving angle of the main roof and the extent of face advance in-between, in all the four workings, revealed that the nature of caving and the support loading depended on the magnitude of the caving angle, viz., lower caving angle with large face advance resulted in the delayed caving and intensive loading on the supports. The field observations of Working 'C' was in good agreement of such mechanism, where the first angle of caving of the main roof was 34°, and the extent of face advance was 15 m.
- The critical rate of face convergence in Workings 'A', 'B', 'C', and 'D' was identified as 4, 21, 8, and 10 mm/m, respectively. The maximum rate of face convergence in Working 'B' confirmed the en masse caving and yielding of face support in response to the heavy weighting event.
- Due to the presence of a thick sandstone roof near the seam, the support deployed at the Workings 'C' and 'D' were overloaded. The load-time step chart showed that the support deployed in the Working 'C' was under-rated as it suffered extreme loading in most of the mining cycles.
- The observations of failure at the face suggested that the face instability mechanism was dominated by shear failure. The pattern of failure zone and the horizontal deformation at the modeled longwall faces revealed that

the stability of the face primarily depended on the stress concentration and the working depth of the mine. The deformation pattern of coal face showed that the horizontal movement initiated at the face center and gradually propagated towards its corner, in the majority of the cases.

- For the assessment of the face instability mechanism, the threshold value of the axial strain in Workings 'A', 'B', and 'D' was identified as 0.5, 0.7, and 0.26%, respectively, based on the depth of failure in the coal walls. On the basis of stress–strain relationship, the point of inflection between the elastic and the plastic regions was identified for Workings 'C' and 'D', which confirmed that the face would behave elastically beyond this point due to an increase in confining stress over the vertical stress.

Acknowledgements The authors are thankful to the Head, Department of Mining Engineering, Indian Institute of Technology (BHU) Varanasi, for providing necessary laboratory facilities for the numerical simulation studies. The authors are grateful to the management of the various longwall mines for their cooperation in the compilation of necessary data pertinent to this study. The views and findings expressed in this paper are the opinions of the authors and not necessarily of the organization which they serve.

Compliance with Ethical Standards

Conflict of interest The authors declare that they have no conflict of interest.

References

Arioglu E, Yuksel A (1984) Design curves for hydraulic face supports. J Min Met Fuels 4–5:173–178

Bai Q, Tu S, Li Z, Tu H (2015) Theoretical analysis on the deformation characteristics of coal wall in a longwall top coal caving face. Int J Min Sci Technol 25(2):199–204

Bai QS, Tu SH, Chen M, Zhang C (2016) Numerical modeling of coal wall spall in a longwall face. Int J Rock Mech Min Sci 88:242–253

Banerjee G, Kumbhakar D, Ghosh N, Yadava KP (2016) Assessment of cavability and categorization of coal measure roof rocks by parting plane approach. In: Proceedings of international conference on recent advances in rock engineering, NIRM, Bengaluru, pp 302–08

Barczak TM, Conover DP (2002) The NIOSH shield hydraulic inspection and evaluation of leg data (SHIELD) computer program. In: Proceedings of 21st international conference on ground control in mining, Morgantown, WV, USA, pp 27–33

Bilinski A, Konopko W (1973) Criteria for choice and use of powered supports. In: Proceedings of the symposium on protection against roof falls, Katowice, Paper No. IV-1

Chen J (1998) Design of powered supports for longwall mining. Dissertation, West Virginia University, Morgantown, WV, USA

Cheng H (1998) Analysis of powered supports resistance and roof behavior. Dissertation, West Virginia University, Morgantown, WV, USA

Das SK (2000) Observations and classification of roof strata behavior over longwall coal mining panels in India. Int J Rock Mech Min Sci 37:585–597

Deb D (1998) Development of the longwall strata control and maintenance system (LOSCOMS). Dissertation, University of Alabama, USA

Deb D, Verma AK (2004) Ground control problems in Indian longwall mines- a perspective and future research outlook. J Min Met Fuels 52(9 & 10):178–185

Frith RC, Creech M (1997) Face width optimisation in both longwall and shortwall caving environments. ACARP Project No. 5015 (accessed)

Ghose AK, Dutta D (1987) A rock mass classification model for caving roofs. Int J Min Geol Eng 5(3):257–271

Ghosh AK (2003) Why longwall in India has not succeeded as in other developing countries like China. Inst Eng (I) J-MN 84:1–4

Guo WB (2015) Stability of coal wall and interaction mechanism with support in fully mechanized working face with great mining height. Dissertation, China University of Mining and Technology

Henderson PG (1980) Experience in longwall mining at Coalbrook Collieries. J South Afr Inst Min Metall 1980:22–36

Hoyer D (2012) Early warning of longwall cavities using LVA software. In: Proceedings of 12th coal operators' conference, University of Wollongong and AUSIMM, pp 69–77

Islavath SR, Deb D, Kumar H (2016) Numerical analysis of a longwall mining cycle and development of a composite longwall index. Int J Rock Mech Min Sci 89:43–54

Itasca (2015) FLAC-3D Version 5.01 User's Manual. Itasca Consulting Group Inc., Minneapolis

Kang H et al (2018) A physical and numerical investigation of sudden massive roof collapse during longwall coal retreat mining. Int J Coal Geol 188:25–36

Khanal M, Adhikary D, Balusu R (2012) Assessment of chock capacity and strata caving for a longwall mine. Geotech Geol Eng 30:395–405

Kong DZ, Wu GY, Ma ZQ, Liu Y (2017) Development and application of a physical model for longwall coal face failure simulation. Int J Min Miner Eng 8:131–143

Kong DZ, Cheng ZB, Zheng SS (2019) Study on the failure mechanism and stability control measures in a large-cutting-height coal mining face with a deep-buried seam. Bull Eng Geol Environ 2019:1–15. https://doi.org/10.1007/s10064-019-01523-0

Le TD, Oh J, Hebblewhite B, Zhang C, Mitra R (2018) A discontinuum modelling approach for investigation of longwall top coal caving mechanisms. Int J Rock Mech Min Sci 106:84–95

Le TD, Zhang C, Oh J, Mitra R, Hebblewhite B (2019) A new cavability assessment for longwall top coal caving from discontinuum numerical analysis. Int J Rock Mech Min Sci 115:11–20

Li Z, Xu J, Yu S, Ju J, Xu J (2018) Mechanism and prevention of a chock support failure in the longwall top-coal caving faces: a case study in Datong coalfield, China. Energies 11(288):1–17

Liu C, Li H, Mitri H (2019) Effect of strata conditions on shield pressure and surface subsidence at a longwall top coal caving working face. Rock Mech Rock Eng 52(5):1523–1537

Majumdar S (1986) The support requirement at a longwall face—a bending moment approach. In: Proceedings of the 27th US symposium on rock mechanics: key to energy production, The University of Alabama, Tuscaloosa, Alabama, pp 325–32

Medhurst TP, Reed K (2005) Ground response curves for longwall support assessment. Min Technol (Trans. Inst Min and Metall A) 114:A81–A88

Mohammadi S, Ataei M, Kakaie R (2018) Assessment of the importance of parameters affecting roof strata cavability in mechanized longwall mining. Geotech Geol Eng 36:2667–2682

Obert L, Duvall WI (1967) Rock mechanics and the design of structures in rock. Wiley, New York

Pan BN, Prasad N (1999) Experience with the operation of powered support longwall face in SECL with particular reference to Balrampur. J. Min. Met. Fuels, SECL Number, pp 126–130

Park DW, Deb D (1999) Longwall strata control and maintenance system—a stethoscope for longwall mining. Mineral Eng 51(10):49–53

Pawlowicz K (1967) Classification of rock cavability of coal measure strata in upper Silesia coalfield. Prace GIG, Komunikat, No. 429, Katowice **(in Polish)**

Peng SS (1998) What can a shield leg pressure tell us? Coal Age 1998:54–57

Peng SS (2006) Longwall mining, 2nd edn. Society for Mining, Metallurgy, and Exploration, Inc. (SME), Englewood

Peng SS, Wu J, Li HC, Chen SL (1986) How to determine yield load of longwall roof supports? Coal Min 10:40–43

Peng SS, Hsiung SM, Jiang JM (1987) Method of determining the rational load capacity of shield supports at longwall faces. Min Eng 197:161–167

Peng SS, Zhu DR, Jiang YM (1989) Roof classification and determination of the support capacity for the fully mechanized longwall faces. In: Special number for longwall mining developments. J Min Met Fuels 1989:289–296

Prusek S, Plonka M, Walentek A (2016) Applying the ground reaction curve concept to the assessment of shield support performance in longwall faces. Arab J Geosci 9:167

Qian M, Miao X, He F (1994) Analysis of key block in the structure of voussoir beam in longwall mining. J China Coal Soc 31(6):557–563 **(in Chinese)**

Qian MG, Shi PW, Xu JL (2010) Mining pressure and strata control. China Mining University Press, Xuzhou **(in Chinese)**

Rezaei M, Hossaini MF, Majdi A (2015a) Determination of longwall mining-induced stress using strain energy method. Rock Mech Rock Eng 48:2421–2433

Rezaei M, Hossaini MF, Majdi A (2015b) Development of a time-dependent energy model to calculate the mining-induced stress over gates and pillars. J Rock Mech Geotech Eng 7(3):306–317

Sandford J, Mahoney S, Conover DP (1999) Shield monitoring to forecast severe face weighting at the South Bulga Colliery, NSW, Australia. In: Proceedings of 18th international conference on ground control in mining, Morgantown, WV, USA, pp 164–175

Sarkar SK (1998) Mechanized longwall mining - the Indian experiences. Oxford and IBH Publishing Company Private Limited, New Delhi

Sarkar SK, Dhar BB (1993) Strata control failures at caved longwall faces in India-experience from Rana to Churcha (1964 to 1990). In: Proceedings of the 4th Asian mining, MGMI Calcutta, pp 361–80

Shabanimashcool M, Li CC (2012) Numerical modelling of longwall mining and stability analysis of the gates in a coal mine. Int J Rock Mech Min Sci 51:24–34

Shabanimashcool M, Jing L, Li CC (2014) Discontinuous modelling of stratum cave-in in a longwall coal mine in the Arctic Area. Geotech Geol Eng 32:1239–1252

Sheorey PR (1994) A theory for in situ stresses in isotropic and transversely isotropic rock. Int J Rock Mech Min Sci Geomech Abstr 31:23–34

Sheorey PR, Mohan GM, Sinha A (2001) Influence of elastic constants on the horizontal in situ stress. Int J Rock Mech Min Sci Geomech Abstr 38:1211–1216

Singh TN, Singh B (1979) Design of support system in caved longwall faces. In: Proceedings of colloquium on longwall face supports, Dhanbad, pp 79–85

Singh TN, Singh B (1982) Design criteria of face supports. In: Proceedings of symposium on state of the art of ground control in longwall mining and mining subsidence (organized by Society of Mining Engineers, New York), pp 145–150

Singh GSP, Singh UK (2004) Cavability assessment model for longwall workings in India. In: Proceedings of the third Asian rock mechanics symposium, Kyoto, pp 295–300

Singh GSP, Singh UK (2009) A numerical modeling approach for assessment of progressive caving of strata and performance of hydraulic powered support in longwall workings. Comput Geotech 36(7):1142–1156

Singh GSP, Singh UK (2010a) Numerical modeling study of the effect of some critical parameters on caving behavior of strata and support performance in a longwall working. Rock Mech Rock Eng 43:475–489

Singh GSP, Singh UK (2010b) Prediction of caving behaviour of strata and optimum rating of hydraulic powered support for longwall workings. Int J Rock Mech Min Sci 47(1):1–16

Smart BDG, Aziz N (1986) The influence of caving in the Hirst and Bulli Seams on powered support ratings. In: Proceedings of the ground movement and control related to coal mining symposium on Wollongong, Australia, pp 182–193

Song G, Chugh YP (2018) 3D analysis of longwall face stability in thick coal seams. J South Afr Inst Min Metal 118:131–142

Suchowerska AM, Merifield RS, Carter JP (2013) Vertical stress changes in multi-seam mining under supercritical longwall panels. Int J Rock Mech Min Sci 61:306–320

Suchowerska AM, Carter JP, Merifield RS (2014) Horizontal stress under supercritical longwall panels. Int J Rock Mech Min Sci 70:240–251

Tadisetty S, Matsui K, Shimada H et al (2006) Real time analysis and forecasting of strata caving behavior during longwall operations. Rock Mech Rock Eng 39(4):383–393

Trueman R, Lyman G, Cocker A (2009) Longwall roof control through a fundamental understanding of shield–strata interaction. Int J Rock Mech Min Sci 46(2):371–380

Unrug K, Szwilski A (1980) Influence of strata control parameters on longwall mining design. In: Proceedings of the 21st US symposium on rock mechanics, Morgantown, Rolla, pp 720–728

Vakili A, Hebblewhite BK (2010) A new cavability assessment criterion for longwall top coal caving. Int J Rock Mech Min Sci 47(8):1317–1329

Verma AK, Deb D (2010) Longwall face stability index for estimation of chock-shield pressure and face convergence. Geotech Geol Eng 28:431–445

Verma AK, Kishore K, Chatterjee S (2016) Prediction model of longwall powered support capacity using field monitored data of a longwall panel and uncertainty-based neural network. Geotech Geol Eng 34:2033–2052

Wang C, Zhang C, Zhao X, Liao L, Zhang S (2018) Dynamic structural evolution of overlying strata during shallow coal seam longwall mining. Int J Rock Mech Min Sci 103:20–32

Wilson AH (1975) Support requirements on longwall faces. Min Eng 1975:479–488

Wilson AH (1980) The stability of underground workings in the soft rocks of the coal measures. Ph.D. Dissertation, University of Nottingham, UK

Yang SL, Wang JC, Yang JH (2017) Physical analog simulation analysis and its mechanical explanation on dynamic load impact. J China Coal Soc 40:1361–1367

Yang S, Song G, Kong D (2019) An evaluation of longwall face stability in thick coal seams through a basic understanding of shield-strata interaction. J Geophys Eng 2019:1–11

Yu B (2014) Study on strong pressure behavior mechanism and roof control of fully mechanized top coal caving in extra thickness

seam in Datong coal mine. Ph.D. Dissertation, China University of Mining and Technology, Xuzhou, China
Zamarski B (1970) Control of roof in longwall faces of Ostrava-Karvina Coal Basin. Report of Coal Research Institute, Ostrava, p 11
Zhao HZ (1985) A study of strata behaviour and support resistance of a fully mechanized longwall face. In: Proceedings of international symposium on mining technology and science, China Institute of Mining and Technology, Xuzhou, Beijing. China Coal Industry Publishing House, pp 67–73